ISSN No. 0737-5352-63

Observed and Calculated Properties of Mid-Level, Mixed-Phase Clouds

Curtis J. Seaman
Thomas H. Vonder Haar

This work was supported by the NASA CloudSat Data Processing Center grant number NAS5-99237. Partial support was also provided by the DoD Center for Geosciences/Atmospheric Research under Cooperative Agreement from the Army Research Laboratory (DAAD01-98-2-0078, DAAD19-01-2-0018 and DAAD19-02-2-0005).

CIRA Cooperative Institute for Research in the Atmosphere

Center for Geosciences/Atmospheric Research

Colorado State University

THESIS

OBSERVED AND CALCULATED PROPERTIES OF MID-LEVEL, MIXED-PHASE CLOUDS

Submitted by
Curtis J. Seaman
Department of Atmospheric Science

In partial fulfillment of the requirements
for the Degree of Masters of Science
Colorado State University
Fort Collins, Colorado
Fall 2003

ABSTRACT OF THESIS

OBSERVED AND CALCULATED PROPERTIES OF MID-LEVEL, MIXED-PHASE CLOUDS

The University of Wyoming King Air research aircraft was flown into five mid-level clouds that formed over the western Great Plains during the Ninth Complex Layered Cloud Experiment (CLEX-9). Four of the clouds were mixed-phase. This study presents the direct observations made of these clouds as well as the cloud properties that were derived from these observations. In particular, profiles of temperature, water vapor mixing ratio, liquid water content (LWC) and ice water content (IWC) are shown. These profiles were used to calculate profiles of latent heating rate, and long- and shortwave radiative heating rate. In-cloud temperatures were observed between +2 °C and –25 °C. Maximum horizontally averaged LWC and IWC values were between 0.04 – 0.28 g m^{-3} and 0 – 0.16 g m^{-3}, respectively. Cloud depths ranged from 248 m to 3106 m, with cloud bases between 2.9 and 5.6 km above mean sea level. Direct observations of ice particles made through the use of 2D-C and 2D-P optical imaging probes were analyzed using the methods of Heymsfield et al. (2002) to account for departures from sphericity, which reduces the observed ice water content by as much as 95%. These methods were also used to fit the observed ice particle size distribution into a modified gamma distribution equation, from which the ice particle effective radii were determined. Knowledge of the ice particle effective radii, plus observations of the liquid droplet effective radii made by a Forward Scattering Spectrometer Probe, were used with the

profiles of LWC and IWC to calculate liquid and ice water paths and optical depths of these clouds. Ice particle size distributions and profiles of IWC show evidence of growth by the Wegener-Bergeron-Findeisen mechanism and aggregation. This data was input into a simple model to calculate the relative importance of subsidence, radiation, entrainment and precipitation in affecting cloud lifetimes. Results of this model show that subsidence and precipitation are the most important processes. It is also shown that the passage of potential vorticity anomalies may be intricately linked to the lifetimes of isolated, non-frontal and non-orographic mid-level clouds. A selection of previous studies was examined in light of these results to develop a consistent picture of the lives of mid-level clouds. The results of this study are shown to be similar to the results of previous studies of mid-level clouds, particularly those that took place over the continental United States.

Curtis J. Seaman

Department of Atmospheric Science

Colorado State University

Fort Collins, Colorado 80523

Fall 2003

ACKNOWLEDGMENTS

This work would not have been possible were it not for the following people: my advisor, Tom Vonder Haar, for giving me this opportunity; my committee members, Steve Rutledge, Mahmood Azimi, and John Davis, for giving me advice, assistance and prodding; Adam Kankiewicz, for providing the satellite imagery; Larry Carey for organizing and managing the CLEX-9 field campaign and gathering the data; the University of Wyoming for providing the aircraft, crew and pilots that gathered the data; the research group at NCAR under the charge of Andy Heymsfield for providing the ice water content analysis and ice particle size distributions; the members of my research group: Jim Jones, Ben Ruston, Kim Mueller, Julie Demuth, Rich Moore, Cathy Meyer, Brian McNoldy and Tomoko Koyama for providing a unique working environment and friendships; and the federal government, particularly the National Aeronautics and Space Administration and the Department of Defense Center for Geosciences/Atmospheric Research, for providing the funding for this study.

This work was supported by the NASA CloudSat Data Processing Center grant number NAS5-99237. Partial support was also provided by the DoD Center for Geosciences/Atmospheric Research under Cooperative Agreement from the Army Research Laboratory (DAAD01-98-2-0078, DAAD19-01-2-0018 and DAAD19-02-2-0005).

Table of Contents

1. Introduction

Literature on the topic of mid-level clouds is sparse, relative to literature on cirrus, boundary layer stratus, stratocumulus and deep convective clouds. Boundary layer stratus and stratocumulus clouds (especially in marine and Arctic environments) are quite persistent, making them relatively easy targets for direct aircraft observations. Deep convective clouds are an important part of the global precipitation rate and the severe weather they produce poses a threat to human (and non-human) life. Although deep convection may produce mid-level clouds, it is not the mid-level clouds that attract most storm chasers. The radiative importance of cirrus clouds has been well documented (e.g. Stephens et al. 1990, McFarquhar et al. 2000) and continues to be studied as questions linger about the role of clouds in climate change. In comparison, mid-level clouds are not often very persistent, are usually mixed-phase, and thin. They do not produce severe weather of their own, and rarely produce precipitation that reaches the ground (Gedzelman 1988). The mixed-phase nature of mid-level clouds and their interactions with their environment and with radiation make them complex, and not much is known about their role in climate. They are not well represented or forecast by current operational forecast models (Vonder Haar et al. 1997), which makes planning a research experiment to study them difficult. If we know more about what makes mid-level clouds "tick", perhaps we will be able to forecast them more reliably, and the more we know about their radiative properties, the more we will know about the role of these clouds in climate. What follows is a description of five mid-level clouds observed during the ninth Complex Layered Cloud Experiment (CLEX-9, Carey et al. to be published), with particular attention given to the microphysical and radiative properties that were

observed or derived from *in-situ* aircraft measurements, and to how these five clouds relate to the mid-level clouds of previous studies (i.e. Fleishauer et al. 2002, Tulich and Vonder Haar 1998, Heymsfield et al. 1991). First, let us review our current state of knowledge about mid-level clouds, based on the studies of the past.

1.1 Overview of Mid-level, Mixed-phase Clouds

Mid-level clouds cover nearly 22% of the earth's surface (Warren et al. 1988). They exist entirely above the boundary layer, which means they are not as closely tied to the surface as boundary layer stratus and stratocumulus. They often contain both liquid droplets and ice particles, which separates them from warm (all liquid) clouds and cirrus clouds (generally all ice) in their morphology and in their radiative properties. Altocumulus clouds are the most likely to produce iridescence and coronas (Gedzelman 1988), and lest we ignore the scientific importance of these clouds (to be outlined below), we still may consider them on their aesthetic appeal.

The radiative and, hence, climatic importance of mixed-phase clouds is not well known at the present and has been a subject of recent research. Sun and Shine (1994) reported that changing the microphysics of a cloud from all liquid to all ice, using their prescribed conditions, changed the optical depth from 28.2 to 2.9, and correspondingly changed the albedo from 72.6% to 29.8%. In another study, Sun and Shine (1995) reported that the inclusion of mixed-phase clouds in a radiative-convective model offset the increase in equilibrium surface temperature due to a doubling of atmospheric CO_2 by as much as 25%, although this number changed according to how the liquid and ice particles were mixed. Their three different simulations assumed 1) ice particles and liquid droplets were uniformly mixed, 2) ice particles existed in a layer above liquid

droplets or 3) ice particles existed in a column next to a column of liquid droplets. Of the clouds presented here and in many other studies of mixed-phase clouds (e.g. Fleishauer 2001, Field 1999, Heymsfield et al. 1991), it was observed that maximum ice water contents (IWC) occurred near cloud base and maximum liquid water contents (LWC) were observed higher in the clouds, making extension of the results of Sun and Shine (1995) to real clouds difficult. Fleishauer (2001) examined the impact of reversing the locations of liquid and ice on radiative heating rate profiles and found that, by assuming the ice phase exists at cloud top, the net radiative cooling was reduced by as much as 5 K hr^{-1}. This would have a significant impact on cloud morphology as simulated by operational forecast models and general circulation models (GCMs).

Fowler and Randall (1996) investigated the role of mixed-phase clouds in the Colorado State University General Circulation Model (CSU GCM). The CSU GCM assumes that water phase is temperature dependent such that any cloud particle existing below –20 °C is ice (Fowler et al. 1996). Liquid and ice cloud particles may coexist in temperatures between –20 °C and 0 °C. In comparison, Heymsfield and Miloshevich (1993) found that, in clouds dominated by homogeneous nucleation, ice particles were found to exist only at temperatures below -30 °C. By varying the CSU GCM to allow supercooled water to exist at temperatures as low as –40 °C, Fowler and Randall (1996) found the globally averaged outgoing longwave radiation (OLR) was reduced by 4.9 W m^{-2}. The impact of doubling atmospheric CO_2 concentrations was compared in twelve GCMs, with globally averaged surface temperature increases ranging between 1.5 °C and 5.5 °C, with variations largely due to the different parameterizations of cloud properties used in the different models (Cess et al. 1993). Clouds remain one of the great unknowns in climate studies.

Mid-level clouds have been known to interfere with military operations, such as during Operation Desert Storm (Vonder Haar et al. 1997). Mid-level clouds routinely

obscured military targets and inhibited the use of Uninhabited Aerial Vehicles, which fly at these altitudes. Aircraft refuelings, which usually take place at altitudes between 3000 and 5500 m, had to be cancelled due to mid-level cloudiness. The inability of operational forecast models to predict the occurrence of mid-level clouds was noted during the Gulf War conflict and served as an impetus to fund the CLEX missions. Also, since mid-level clouds routinely contain supercooled liquid droplets, they pose a possible icing hazard for both military and civilian aircraft.

Heymsfield et al. (1991) examined two mid-level clouds (one mixed-phase and one liquid only) that formed over Wisconsin during the First ISCCP[1] Regional Experiment (FIRE, Starr 1987, Cox et al. 1987) cirrus experiment during the fall of 1986. From both aircraft measurements and a simple modeling study, the authors concluded that the clouds were structurally and thermodynamically similar to stratocumulus, and radiation and entrainment were important in the life cycle of these clouds. The clouds existed between 7.1 and 7.9 km above mean sea level (MSL) at temperatures between -25 °C and -30 °C. Maximum net radiative heating rates were less than 24 K day^{-1} and occurred near cloud base and maximum net radiative cooling rates were between 20 and 85 K day^{-1} and occurred near cloud top. This is due to the net absorption at cloud base of longwave radiation emitted by the earth's surface, and the net emission of longwave radiation toward space at cloud top. Radiative heating rates and flux profiles calculated neglected the ice phase, however.

Tulich and Vonder Haar (1998) examined the microphysical, radiative and thermodynamic structures of two mid-level clouds observed over Kansas during the first Complex Layered Cloud Experiment (CLEX-1) in June of 1996. One cloud was primarily comprised of ice particles; the other was primarily comprised of liquid and existed in

---

[1] ISCCP stands for International Satellite Cloud Climatology Project (see Schiffer and Rossow 1983)

several layers. The ice cloud had a structure similar to that of cirrus, and had net radiative heating at cloud base and net radiative cooling at cloud top both less than 5 K day^{-1}. The liquid cloud had a structure similar to that of convective cumulus elements rising into a stratocumulus layer, and had a cloud averaged radiative cooling rate of 0.5 K day^{-1} with weak radiative heating at cloud base and intense radiative cooling at cloud top.

Fleishauer et al. (2002) examined the microphysical properties of six mid-level clouds observed over both Oklahoma and Montana during the fifth Complex Layered Cloud Experiment (CLEX-5) in the fall of 1999 and spring of 2000. A more detailed description of the microphysical properties, as well as examination of the radiative and thermodynamic properties of these clouds can be found in Fleishauer (2001). The mid-level clouds were observed at temperatures between 0 °C and -31 °C at heights between 2.4 and 7.2 km MSL. Five of the clouds were mixed-phase, while one was comprised of liquid only. Two of the clouds existed in multiple layers, both of which were mixed-phase. Unlike marine stratocumulus, the mid-level clouds described by Fleishauer et al. (2002) lacked strong cloud-top inversions and wind shear. The authors speculated that this was due to the fact that the clouds observed did not last long enough to produce a strong temperature inversion and/or such an inversion did not exist when the cloud formed. Wind shears were weak, presumably due to the fact that mid-level clouds are not "tied" to the surface by turbulence and drift with the ambient winds.

1.2 Scientific Objectives

This study may be considered a follow-up to the study of Fleishauer (2001). Aircraft observations of five mid-level, mixed-phase clouds are presented as part of CLEX-9.

Primary emphasis is given to the microphysical and radiative properties of these clouds, with some attention given to thermodynamics. The microphysics of the ice phase was examined using the methods detailed in Heymsfield et al. (2002). Profiles of cloud LWC and IWC, temperature, and water vapor mixing ratio have been developed for each of the case studies presented. These profiles, along with variables derived from these profiles, were used to calculate radiative and latent heating rate profiles. A simple model was used to determine the physical processes most important for maintaining and/or dissipating the clouds.

The main goals of this work are as follows: 1) to quantify the microphysical structure of five mid-level, mixed-phase clouds and compare them to those of previous studies, 2) to determine the role of radiation in the evolution of mid-level, mixed-phase clouds, and 3) to determine the physical processes most important in affecting the lifetime of mid-level, mixed-phase clouds.

This thesis is organized as follows. Chapter 2 presents an overview of the CLEX-9 field experiment, the instrumentation used to collect the data, the data analysis methods and the radiative transfer model used. Chapter 3 details the observed and derived properties of the five mid-level clouds studied and the environment they formed in. These clouds will be compared with each other and with those presented in previous studies (i.e. those mentioned in section 1.1). Chapter 4 discusses the physical processes that are known to affect the lifetime of mid-level clouds and presents the formulation and results of a simple model used to evaluate the importance of each of these processes in the clouds presented. A review of the results and conclusions drawn from this work are presented in Chapter 5 along with proposed areas for future research.

2. Data Collection

In this chapter, we discuss the instrumentation, aircraft flight strategies, and methods used to collect and analyze the data presented in the next chapter. We begin with an overview of the CLEX-9 field project in section 2.1. Section 2.2 discusses the research aircraft used and its instrumentation. Section 2.3 provides an overview of the methods detailed in Heymsfield et al. (2002) used to examine the ice phase microphysics and the methods developed for this study used in data analysis. The BUGSrad radiative transfer model was used in calculation of the radiative heating rate profiles and will be discussed in section 2.4.

2.1 The Ninth Complex Layered Cloud Experiment

The Complex Layered Cloud Experiment (CLEX) is an ongoing DoD (Department of Defense) Center for Geosciences and Atmospheric Research (CGAR) sponsored research program dedicated to understanding the processes inherent in the formation, maintenance, and dissipation of non-orographic, non-precipitating[2], mid-level clouds. This research has also allowed for investigation into the problems of satellite detection (Jones 2003) and forecasting (research in progress) of these clouds.

[2] In this context, "non-precipitating" means precipitation is not observed at the earth's surface. As will be discussed in Chapter 4, these clouds may contain particles large enough to precipitate out of the cloud.

The ninth CLEX intensive observation period occurred in the fall of 2001. The University of Wyoming King Air research aircraft (see section 2.2) was flown through mid-level clouds over western Nebraska and eastern Wyoming. The aircraft was flown in both Lagrangian spirals (i.e., the aircraft spirals around the same cloud parcel as it drifts with the ambient wind) and Eulerian racetracks (i.e., the aircraft flies in loops over the same point on the surface). In addition to the aircraft measurements, ground based measurements were taken from North Platte, NE and included the NOAA-ETL dual frequency microwave radiometer, the CSU micropulse lidar, and short- and long-wave radiation instrumentation (Carey et al. 2001). Radiosondes were launched from North Platte, both at the National Weather Service Office (KLBF), at 00 and 12 UTC, and at the ground instrumentation site before and after aircraft sampling of the clouds. Geostationary and polar orbiting satellite remote sensing data was gathered when available.

2.2 The University of Wyoming King Air

All aircraft data collected for this study came from the University of Wyoming King Air (UWKA) research aircraft (see Figure 2.1). The atmospheric properties measured by the UWKA and used in this study include LWC, temperature, dew point temperature, pressure, altitude, ambient vertical velocity, and liquid droplet effective radius. The instruments used to make these measurements will now be discussed.

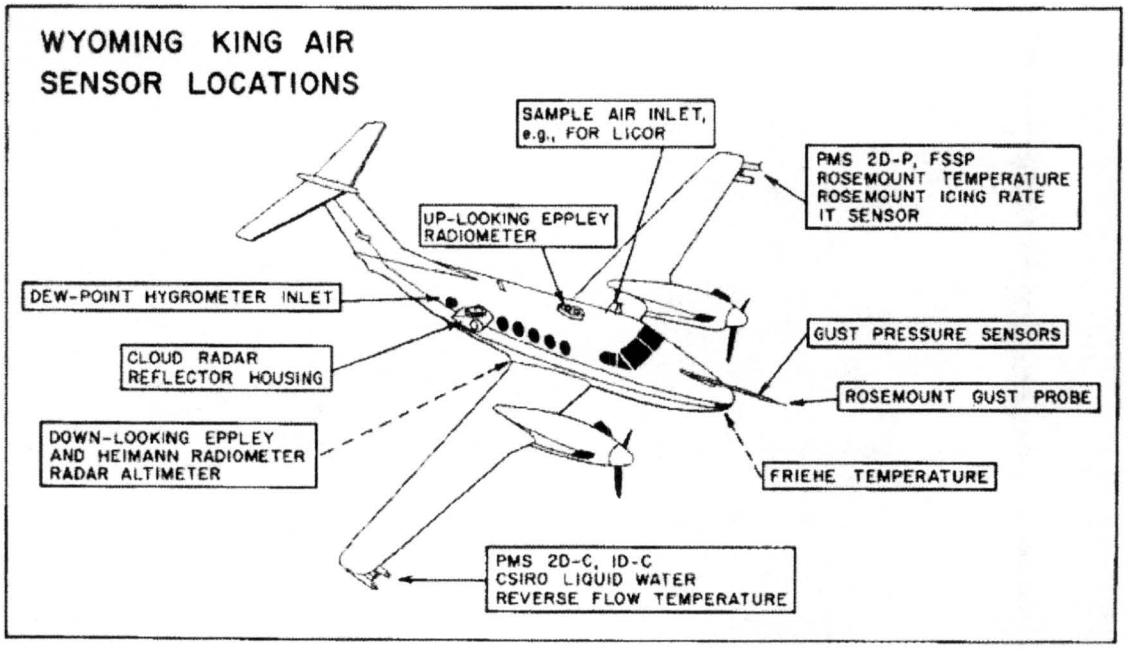

Figure 2.1. The UWKA and the locations of the various sensors. In this study, data were collected from the PMS 2D-C and 2D-P probes, the FSSP probe, the Rosemount temperature sensor, the dew-point hygrometer, and the PVM-100A probe (not shown). Image courtesy of the University of Wyoming.

Measurements of LWC were taken from the Gerber Scientific, Inc. PVM-100A probe (Gerber et al. 1994). This instrument uses a laser-diode light source to irradiate a volume of 1.25 cm^3. Cloud particles enter the laser beam and scatter light into the near-forward direction into a lens that focuses the scattered light onto a variable-transmission filter and sensor for each channel. The flux of light onto the sensors is a function of the particle size distribution, from which the LWC and particle surface area (PSA) can be derived. As reported in Gerber et al. (1994), the filters used allow for a linear relationship between instrument response and LWC for particles between 4 μm and 45 μm in diameter. The response falls off for larger and smaller particles, with LWC underestimated by 50% at 2 μm and 70 μm. Wind tunnel tests reported by Garrett and Hobbs (1999) indicate that LWC is underestimated by 12% in the range from 0 to 0.75 g

m^{-3}, which is the range over which LWC was observed during CLEX-9. Garrett and Hobbs (1999) also report a larger response fall off for particles larger than 20 μm than that reported by Gerber et al. (1994). No attempt was made in this study to correct this underestimation.

Temperature was measured with a Rosemount platinum resistance thermometer. The instrument is accurate to within +/- 0.5 °C at temperatures between +/- 50 °C. The housing of the sensor was heated to eliminate icing effects, although the sensor itself was exposed to hydrometeors, which may introduce errors in cloud due to the wetness of the sensor.

Dew point temperatures were measured using a Cambridge Systems Model 137-C3 hygrometer. In this instrument, light is reflected off of a mirror that is chilled until water or ice condenses on its surface. At that point, the intensity of the reflected light changes, and the temperature of the mirror is the dew point (or frost point if the temperature is below 0 °C). Measurements of the frost point are converted into dew points. The accuracy of this instrument is specified as +/- 2.0 °C over the range of temperatures observed.

The vertical velocity of the ambient air was measured using a Honeywell Laserref SM Inertial Reference System. In this instrument, ring laser gyros and accelerometers are used to determine the aircraft's position, altitude and accelerations. With knowledge of the velocity of the aircraft relative to the ground, wind velocities can be determined. This instrument has a resolution of <1.0 cm min^{-1} and an accuracy of +/- 15 cm s^{-1}.

Liquid droplet effective radius was observed using a PMS Forward Scattering Spectrometer Probe (FSSP, Knollenberg 1981). In this instrument, cloud particles pass through a laser, and the amount of light scattered in the forward direction is detected. This amount is dependent on the size of the particle. The FSSP uses this size information to determine the particle size distributions, total particle concentrations and

LWC. If we denote the particle size distribution as n(r) dr, where r is radius, and assume the particles are spheres, then the total cross-sectional area of the particles per unit volume of air is given by

$$A = \pi \int_0^\infty r^2 n(r) dr \tag{2.1}$$

The total volume of the particles per unit volume of air is given by

$$V = \frac{4}{3} \pi \int_0^\infty r^3 n(r) dr \tag{2.2}$$

The effective radius, r_e, is the ratio of the volume and the area (Stephens 1994):

$$r_e = \frac{V}{A} \tag{2.3}$$

Numerous studies have been performed to evaluate the accuracy and reliability of the FSSP (e.g. Dye and Baumgardner 1984, Tsonis et al. 1987, Baumgardner and Spowart 1990). The main problems with the FSSP are coincidence, dead-time, phase discrimination, and departures from sphericity. When the sample volume of the FSSP contains high concentrations of cloud particles (>300 cm^{-3}), more than one particle may enter the laser beam coincidently and be detected as one large particle. The finite time it takes for the FSSP to process the detection of a particle, called dead-time, allows for particles to pass through the beam undetected. These processes lead to an underestimation of total particle concentration by ~10% in regions of high particle concentration. In this study, FSSP particle concentrations approached, but did not exceed, 300 cm^{-3} during some of the flights. The data has been conditioned as in Brenguier (1989) to correct for coincidence and dead-time errors.

The FSSP is designed to detect particles in the size range from 2 to 47 μm. The relationship between the amount of forward scattered light and particle size is based on the assumption that the particles are spherical, which is appropriate for liquid droplets in this size range. However, the FSSP has no method for discriminating liquid from ice. Any particles detected are assumed to be liquid. Therefore, the detection of any small ice particles, which have a tendency to be slightly non-spherical (Dr. Paul Lawson, personal communication), will introduce errors in calculation of the liquid droplet effective radius given by equation (2.3), although this error is estimated to be less than 10%.

Pressure was measured using a Rosemount 1201F2 static pressure sensor. This model senses pressure using a capacitive sensing capsule. A diaphragm is exposed to the pressure media and a fixed capacitor plate, isolated in a reference vacuum from the capacitive element in the sensing capsule. As pressure is increased, the diaphragm deflects toward the fixed capacitor plate, changing the capacitance of the capsule. This instrument is accurate to within 0.5 mb.

2.3 Processing of Microphysical Data

Ice particle size distributions, ice particle effective radii, and IWC measurements were derived from PMS 2D-C and 2D-P probes using the methods developed by Heymsfield et al. (2002). The 2D-C and 2D-P probes are designed to detect cloud particles in the size ranges 25 μm to 1 cm and 200 μm to 1 cm, respectively. In these instruments, a laser shines on a two dimensional array of photodiodes. As cloud particles pass through the laser beam, they cast a shadow on a number of photodiodes.

The number of photodiodes obscured is related to the particle size. The resolutions of these instruments are 25 μm for the 2D-C and 200 μm for the 2D-P. The calculation of IWC from these instruments is based on the assumption that the particles are spheres, which is a poor assumption for ice particles in these size ranges.

Heymsfield et al. (2002) developed a method for analyzing 2D-C and 2D-P data to account for the non-sphericity of ice particles based on particle habit. The important features of this method will now be discussed. Images of ice particles were collected by the 2D-C and 2D-P probes and analyzed to determine their general habit. The maximum projected dimension, D, and cross-sectional area of the particles are related to the area ratio, a_r, and effective density, ρ_e, based on empirical relationships unique to each particle habit, and described in detail in Heymsfield et al. (2002). The area ratio is defined as the ratio of the cross-sectional area of the particle to the area of a circle with diameter D. The effective density is the mass of the particle divided by the volume of a sphere with diameter D. The effective density is related to a_r, and is used to calculate the IWC. Values of a_r and ρ_e are used with knowledge of the general particle habit to determine the fall speed, which is important for determining precipitation rates, and will be discussed more in chapter 4.

The ice particles detected by the probes were binned based on D for 5-second intervals. Modified gamma distributions were fit to the 5-second samples and were given the functional form

$$n(D) = N_0 D^{\mu} \exp(-\lambda D) \tag{2.4}$$

from which the parameters N_0, λ and μ are determined. The total number of particles per unit volume, N_T, is given by

$$N_T = \int_0^\infty n(D)dD = N_0 \lambda^{-(\mu+1)} \Gamma(\mu+1) \tag{2.5}$$

where $\Gamma(x)$ is the gamma function. The mode radius, r_m, and effective radius, r_e, of the modified gamma distributions are given by

$$\begin{aligned} r_m &= \frac{\mu}{2\lambda} \\ r_e &= \frac{\Gamma(\mu+4)}{2\lambda\Gamma(\mu+3)} \end{aligned} \tag{2.6}$$

From equations (2.2), (2.5), and the definition of r_m in (2.6), the IWC follows as

$$IWC = \frac{4}{3}\pi\rho_e N_T r_m^3 \frac{\Gamma(\mu+4)}{\Gamma(\mu+1)} \tag{2.7}$$

This data was processed at the National Center for Atmospheric Research (NCAR) before its inclusion in this study.

2.4 Radiative Transfer Model

The BUGSrad radiative transfer model was used to calculate radiative heating rate profiles. This model was developed as the radiative transfer portion of the CSU GCM. An overview of the theory, rationale and parameterizations used to develop the BUGSrad model can be found in Stephens et al. (2001) and Gabriel et al. (2001).

BUGSrad allows for the direct input of both the liquid and ice phase particle concentrations. The model uses the two-stream method of solution to calculate radiometric fluxes and heating rates for six spectral bands in the shortwave and twelve in

the longwave. Ritter and Geleyn's (1992) delta-Eddington approximation to the two-stream equation in the shortwave, and the constant hemispheric approximation to the two-stream equation in the longwave are utilized, as well as the adding method of Stephens and Webster (1979). The BUGSrad radiation scheme includes gaseous, cloud, and surface absorption and scattering in a plane-parallel atmosphere. In addition, the scheme uses relations from Stephens et al. (1990) for computing cloud optical properties. The k-distribution from Fu and Liou (1992) and the AER CKD Version 2.1 water vapor continuum data (Clough et al. 1989) are used in the gaseous absorption routines.

Several modifications were made to BUGSrad for this study. A subroutine was added to calculate the solar zenith angle based on latitude, longitude, date and time. The latitude and longitude of North Platte, NE (41.1 ^{o}N, 100.8 ^{o}W) were used in all of the radiative transfer calculations. BUGSrad uses the modified gamma distribution to determine cloud optical properties. As is, the model assumes values of liquid and ice effective radii of 10 μm and 30 μm, respectively, and assumes $\mu = 1$. Values of μ and r_e characteristic of those derived during CLEX-9 were used instead. Sensitivity tests revealed, however, that this modification changed the heating rates by less than 0.5 K day^{-1}, which is much less than the change in heating rates due to uncertainties in the LWC and IWC measurements. The asymmetry parameter was varied over the range of values presented in Takano and Liou (1995) and Gerber et al. (2000). This was found to have a negligible impact on the heating rate calculations.

BUGSrad takes as input profiles of temperature, water vapor specific humidity, and specific liquid and ice water contents using pressure as the vertical coordinate. Specific liquid and ice water contents are simply the LWC and IWC divided by the density of air, which was calculated using the Ideal Gas Law. Water vapor specific humidity was

calculated from the dew point temperature. The dew point temperature, T_d, was related to water vapor pressure, e, using the empirical formula (Bolton 1980)

$$e = 611.2 \exp\left(\frac{17.67 T_d}{T_d + 243.5}\right) \tag{2.8}$$

where e is in Pa and T_d is given in °C. The water vapor mixing ratio, w_v, is given by (Bohren and Albrecht 1998)

$$w_v = \frac{\varepsilon e}{p - e} \tag{2.9}$$

where $\varepsilon = 0.622$ is the ratio between the gas constant for dry air and the gas constant for water vapor and p is the pressure. The water vapor mixing ratio is related to the specific humidity, q_v, by (Bohren and Albrecht 1998)

$$q_v = \frac{w_v}{1 + w_v} \tag{2.10}$$

The 5-second averaged values of temperature, dew point, LWC and IWC from the entire in-cloud portion of the flights were averaged over 2 mb layers in the vertical, which were then converted to profiles of specific liquid and ice water contents and water vapor specific humidity. It was noted that biases in the LWC measurement were evident after averaging on several of the flight days. This resulted in LWCs as large as 0.01 g m^{-3} being measured outside of the cloud. When these biases occurred, their average value was computed and subtracted from the LWC profile. This data was merged with similar data from the North Platte National Weather Service radiosondes launched at 12 UTC on each of the flight days and input into BUGSrad.

3. Observed Cloud Properties

This chapter presents the properties that were observed in five mid-level clouds sampled by the UWKA during CLEX-9. Each of these case studies will include a brief discussion of the synoptic scale environment that the clouds formed in, an overview of the cloud's morphology and lifetime, and a description of the vertical structure of hydrometeors, and infrared (LW), solar (SW) and latent heating rates. The last section of this chapter (section 3.6) is dedicated to characterizing the radiative properties that are useful for cloud modeling and remote sensing studies. This data is also compared to and contrasted against the results of previous studies of mid-level clouds (i.e. those mentioned in Section 1.1), in an effort to gain insight into the similarities and differences that exist among mid-level clouds.

3.1 14 October 2001

The cloud field observed on 14 October formed during the overnight hours in northwesterly flow on the back edge of a mid-level shortwave trough that passed over Nebraska the previous day. The UWKA sampled the cloud field from 1215 UTC until 1610 UTC. Hourly IR satellite images during this time period, along with the aircraft flight path, are shown in Figure 3.1. Sunrise occurred at 1352 UTC at North Platte, NE, which is located on the eastern edge of the cloud field.

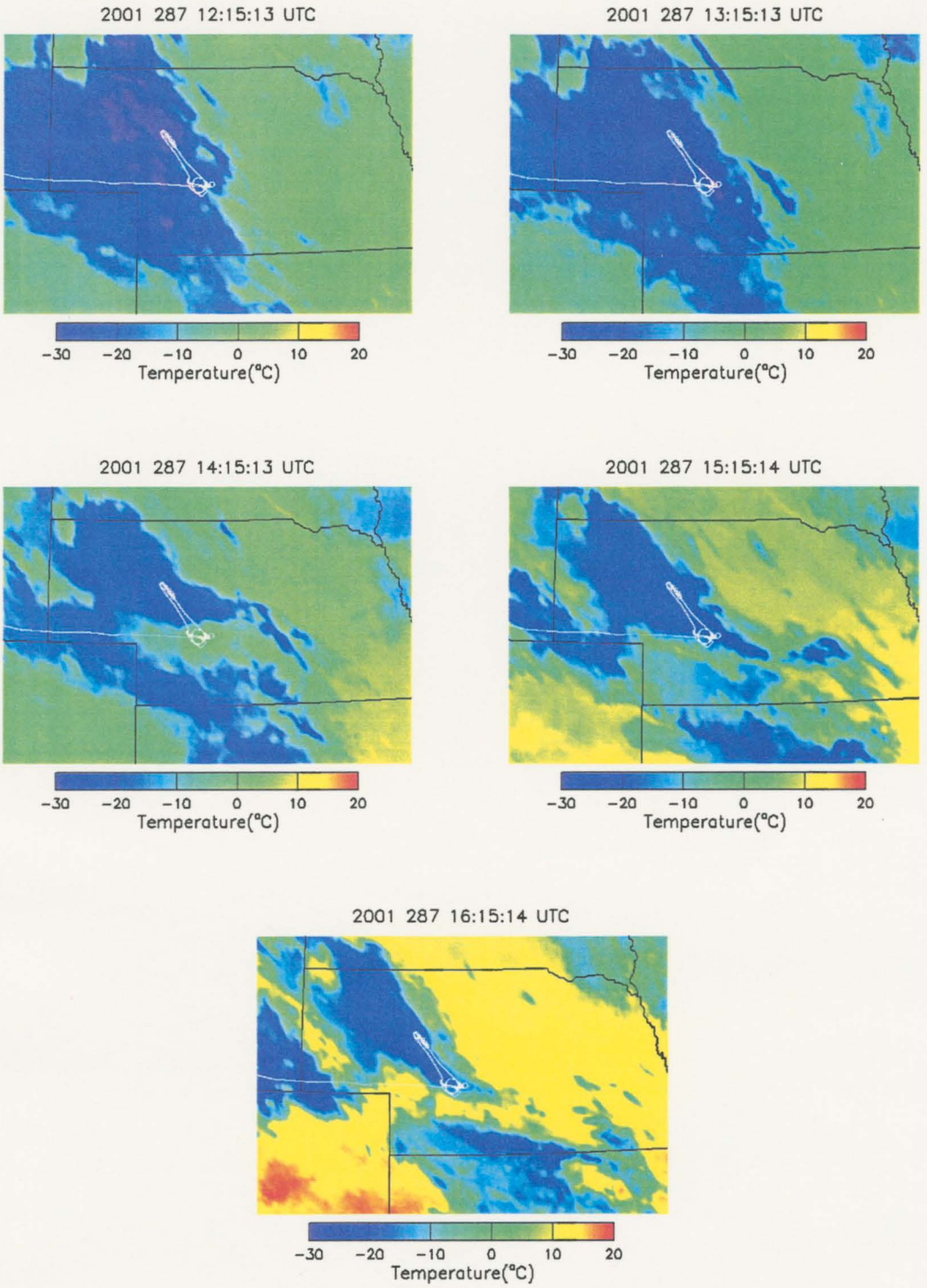

Figure 3.1. Hourly IR satellite images of the 14 Oct cloud field during the in-flight time of the UWKA. IR brightness temperatures are plotted on a Celsius scale. Also plotted is the entire flight path of the UWKA during this time period.

The UWKA flew beneath the cloud for the first leg of the flight over eastern Wyoming and the Nebraska Panhandle. During this time significant amounts of ice were observed, below the visible base of the cloud. Figure 3.2 shows the profile of LWC and IWC observed during the remainder of the flight. The maximum LWC was 0.1 g m^{-3} and occurred just below cloud top. The NCAR IWC analysis shows an absence of ice in the main cloud layer. This is in sharp contrast with the profile of IWC given by the 2D-C probe, which observed horizontally averaged IWCs as high as 0.15 g m^{-3}. Given that this cloud contained mostly aggregates, and that ρ_e for aggregates is typically less than 0.05 g cm^{-3} (Heymsfield et al. 2002), the 2D-C probe was overestimating the IWC by a factor of 15-20. This leads to an important point: accounting for the non-sphericity of ice particles leads to reductions in the measured IWC by as much as 95%. The actual IWC was most likely less than 0.01 g m^{-3}, making this cloud liquid-only for all intents and purposes.

The profiles of LW, SW and latent heating rate profiles at 16 UTC for the 14 Oct cloud are shown in Figure 3.3. Although there was likely ice present that did not show up in the NCAR analysis, the inclusion of the 2D-C IWC corrected for non-sphericity lead to a change in radiative heating rates of less than 10% and a change in the latent heating rate of less than 1%. See the appendix for a detailed description of the calculation of the latent heating rates.

In this study, cloud base and cloud top are defined as the heights (pressures) that form the boundaries of the most significant layers of non-zero LWC and IWC. For example, cloud base and cloud top for the 14 Oct cloud are taken to be 560 mb and 520 mb, respectively (Figure 3.2). Using this definition, the main cloud layer was 458 m thick and centered at 4.9 km MSL. The heating rate profiles (Figure 3.3) indicate a moderate net heating (+12 K day^{-1}) just above cloud base and a strong net cooling (-50 K day^{-1}) just below cloud top. This is consistent with the explanation that there is a net absorption

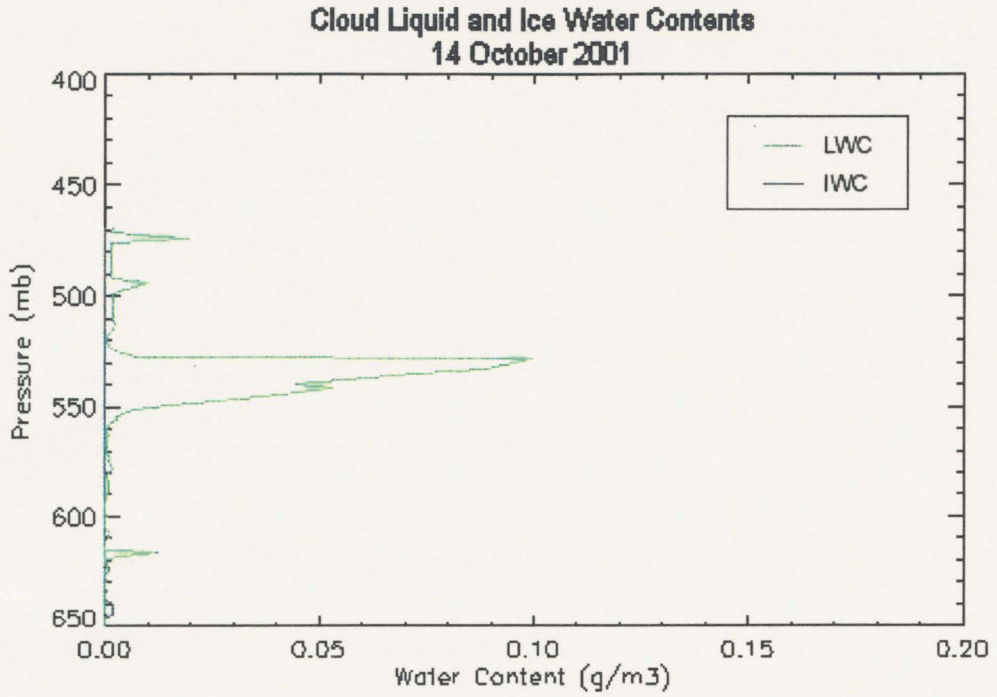

Figure 3.2. Profiles of LWC and IWC for 14 Oct. The IWC of this cloud is negligible.

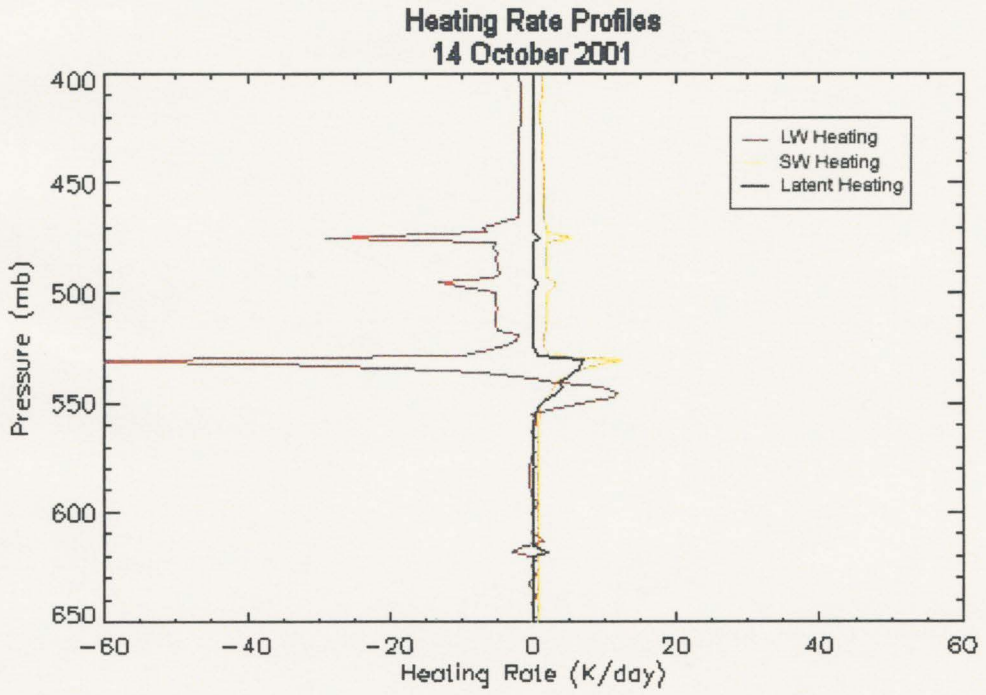

Figure 3.3. Profiles of LW, SW and latent heating rates at 16 UTC for the 14 Oct cloud.

of radiation at cloud base due to longwave emission by the surface and a net emission of longwave radiation out the top of the cloud. The latent heating rate is proportional to the LWC and IWC, and so is a maximum just below cloud top where the maximum LWC is observed. This cloud was thin enough to experience solar heating throughout the cloud layer. The maximum solar heating rate at cloud top is similar in magnitude to the longwave heating at cloud base. The two thin layers of non-negligible LWC above the main cloud layer are radiatively active, with minor solar and latent heating and moderate longwave cooling.

Temperature and water vapor mixing ratio profiles are shown in Figure 3.4. The main cloud layer existed between –19 °C and –22 °C. Two small temperature inversions, both less than 2 °C, existed at 528 mb and at 616 mb. The upper inversion occurred at the height where the LWC of the main cloud begins to rapidly decrease with height, suggesting that this inversion prevented further vertical cloud growth. The two minor layers above the main cloud existed at –23 °C and –25 °C, and were above this inversion. The lower inversion is associated with a peak in the water vapor mixing ratio, which indicates an inversion in the dew point temperature profile. Another thin layer of non-negligible LWC existed at the height of this inversion (see Figure 3.2). Temperatures in this layer were near –11 °C.

The 14 Oct cloud appeared to be convective in nature before sunrise. Generating cells no more than 1 km across existed at cloud top and extended 100 m above the rest of the cloud field. After sunrise, however, the convection slowed and the cloud took on a more stratiform appearance. This is most likely due to the influence of solar radiation. Before sunrise, the SW heating rate is zero and the net cooling rate was more than 60 K day^{-1} at cloud top. Incoming solar radiation after sunrise reduced the net cooling at cloud top by more than 10 K day^{-1} by 16 UTC. This would act to decrease the instability of the

cloud layer that results from the diabatic heating processes shown in Figure 3.3, and would suppress the convection.

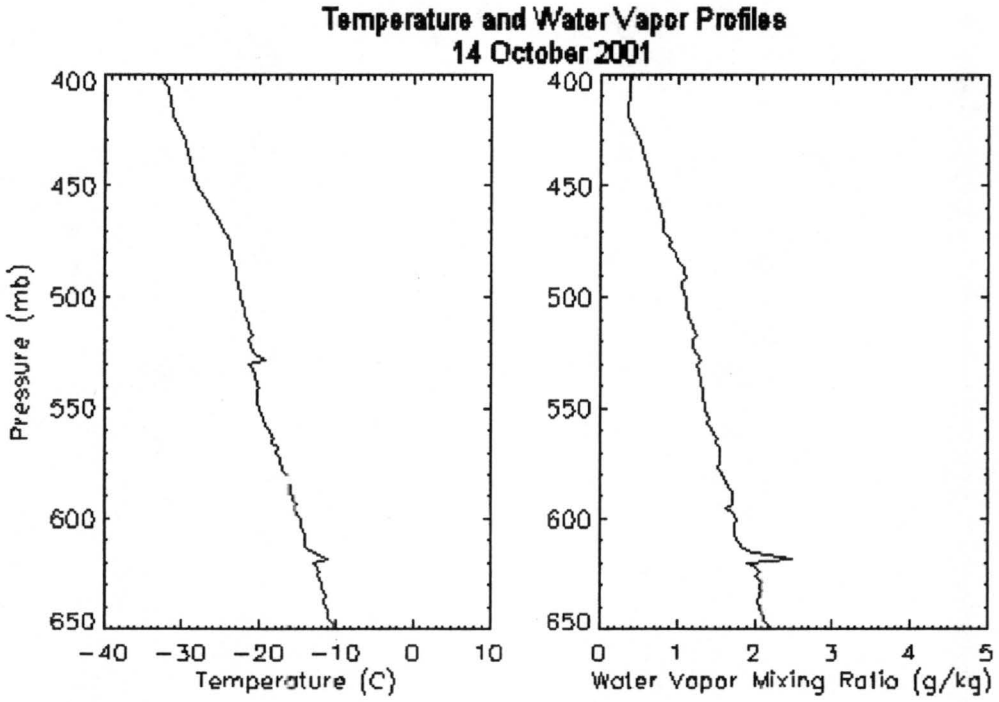

Figure 3.4. Profiles of temperature, left, and water vapor mixing ratio for the 14 Oct cloud. The boundaries of the main cloud layer are near 520 mb and 560 mb.

3.2 19 October 2001

An extensive mid-level cloud field formed during the overnight hours on 19 October 2001 in a region of positive vorticity advection (PVA) that coincided with the left exit region of a jet streak in the upper troposphere. As with the 14 Oct cloud, northwest flow prevailed across the region. The UWKA sampled two different portions of this cloud field at two different altitudes. The portion of the cloud over North Platte, NE was sampled for 75 minutes from 1145 UTC to 1300 UTC. Sunrise at North Platte was 1400 UTC. This

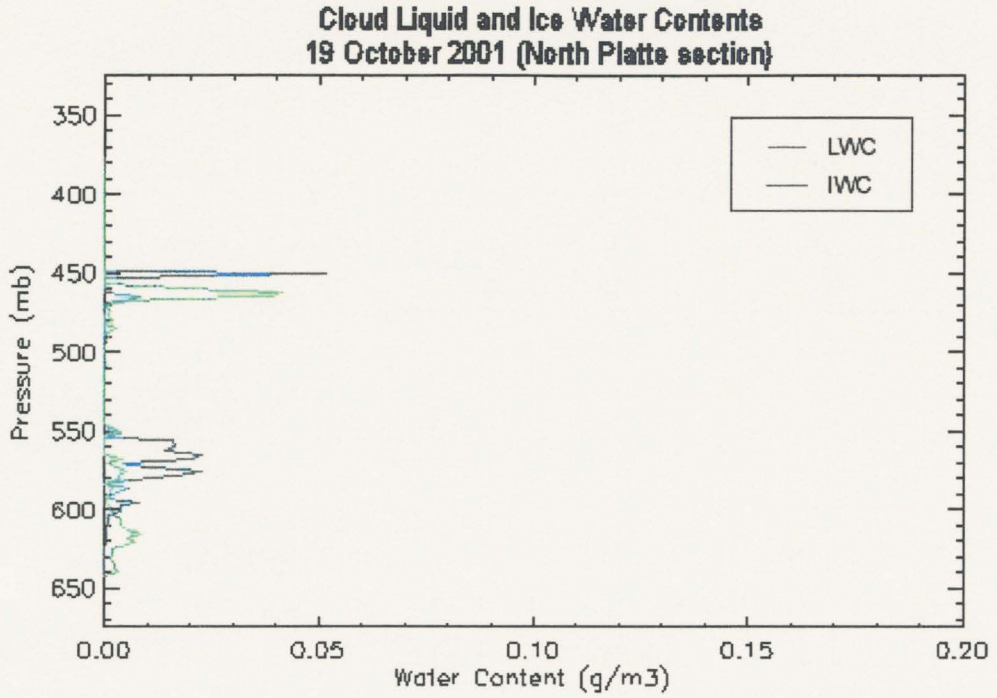

Figure 3.5. Profiles of LWC and IWC for the North Platte section of the 19 Oct cloud.

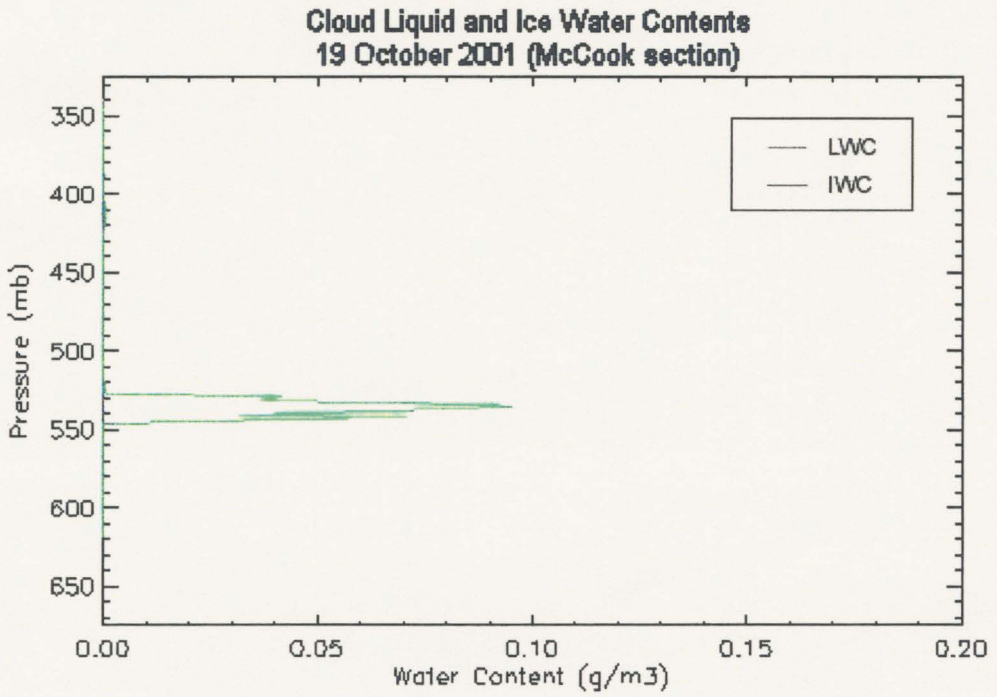

Figure 3.6. Profiles of LWC and IWC for the McCook section of the 19 Oct cloud.

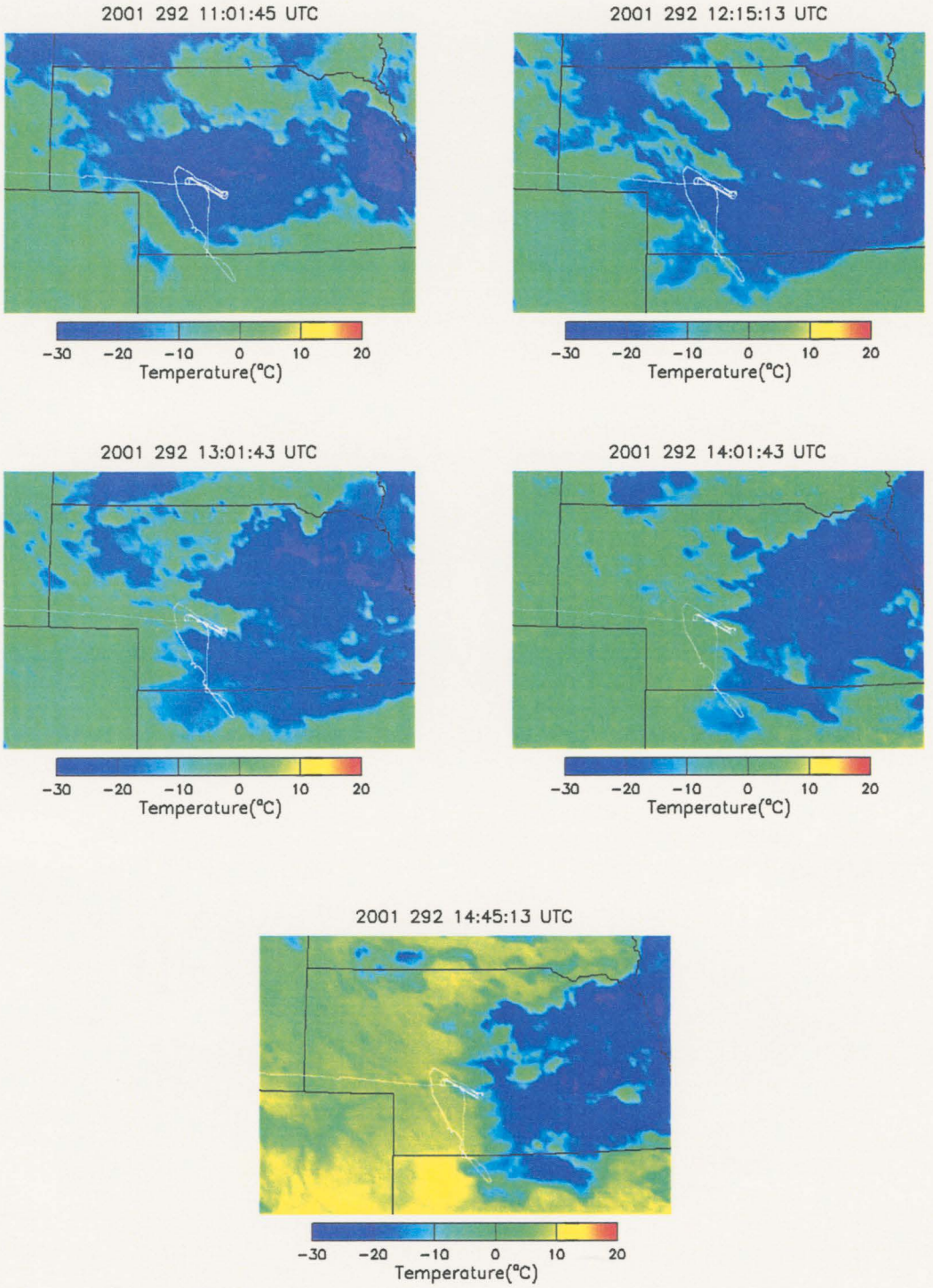

Figure 3.7. Same as Figure 3.1, except for the 19 Oct cloud.

portion of the cloud, hereafter called the North Platte section, consisted of multiple layers of both liquid and ice (Figure 3.5). The aircraft then sampled a portion of the cloud field over SW Nebraska and NW Kansas after sunrise for 25 minutes as it rapidly dissipated. This portion of the cloud, hereafter called the McCook section, consisted almost entirely of liquid droplets and was very thin (Figure 3.6). Figure 3.7 shows IR satellite images of the cloud field during the entire flight of the UWKA along with the flight path. The western portion of the cloud field rapidly dissipated after sunrise, although the satellite imagery suggests the cloud was already beginning to dissipate prior to sunrise. The portion of the cloud over eastern Nebraska (not sampled) remained intact, even after sunrise.

The North Platte section was similar to the multi-layer cloud systems discussed in Fleishauer (2001), with ice particles found throughout the vertical extent of the cloud. This section of the cloud was unusual among mid-level clouds in that the upper-most layer, near 450 mb (6.2 km MSL), consisted entirely of ice. Beneath the ice layer was a mixed-phase layer between 455 mb and 470 mb (5.8 - 6.2 km MSL). A deeper mixed-phase layer existed between 545 mb and 640 mb (3.6 – 4.8 km MSL). The horizontally averaged LWC and IWC values were small in each layer, never exceeding 0.06 g m^{-3}. Temperatures ranged from –23 °C at the top of the all-ice layer to –6 °C at the base of the lower mixed-phase layer (Figure 3.8). No significant temperature inversions existed in this section of the cloud, although the top layers of the cloud existed in a nearly isothermal layer that extended up to 415 mb. The lone inversion at 650 mb represents a discontinuity resulting from the merging of the aircraft data with that of the radiosonde sounding.

Heating rate profiles (Figure 3.9) reveal that the North Platte section was thin in a radiative sense. Solar (SW) heating was absent due to the fact that the cloud was sampled before sunrise. There was no IR (LW) heating in any of the cloud layers since the cloud was thin enough, and the LWC and IWC were small enough that the amount of

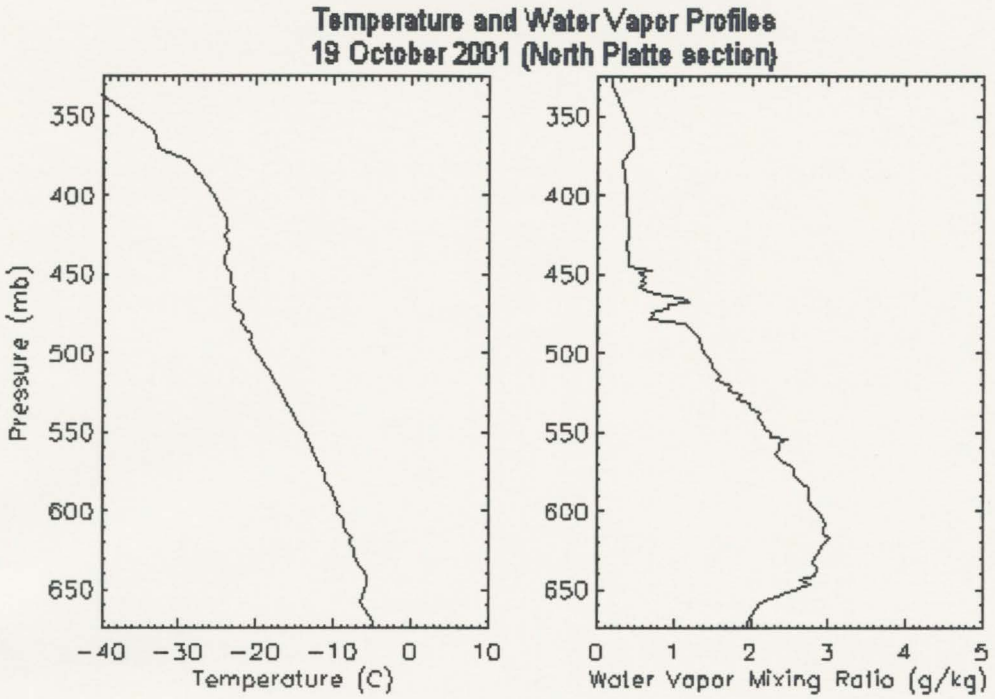

Figure 3.8. Same as Figure 3.4, except for the North Platte section of the 19 Oct cloud. Cloud layers existed between 450 and 470 mb and between 550 and 640 mb.

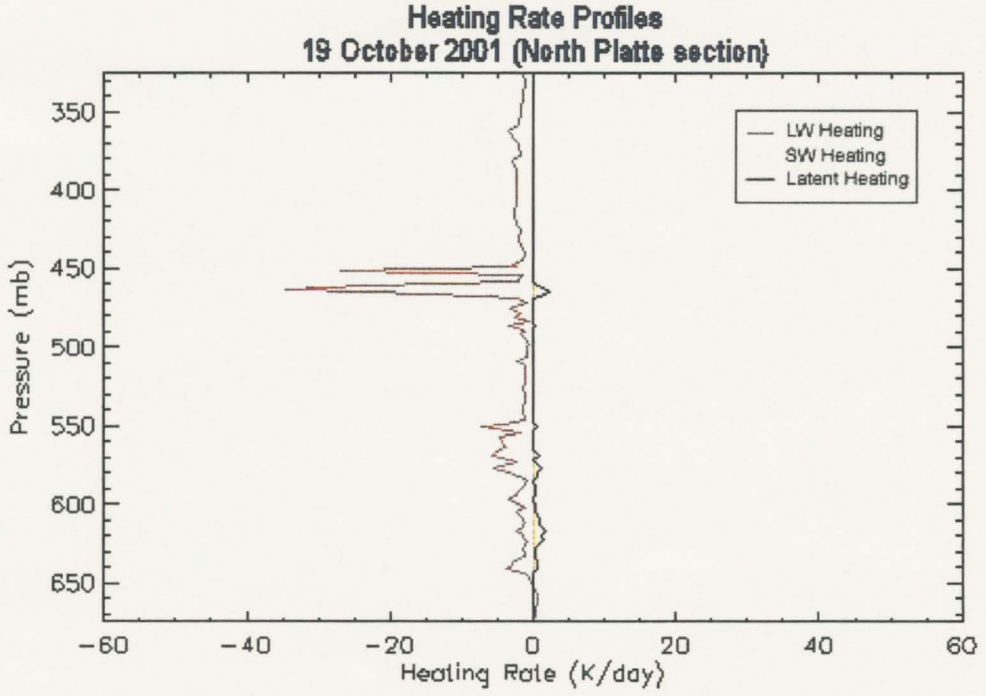

Figure 3.9. Profiles of LW, SW and latent heating rates at 13 UTC for the North Platte section of the 19 Oct cloud.

LW radiation absorbed by the cloud particles was much less than the amount of LW radiation emitted. The small liquid and ice water contents also led to small latent heating rates.

Ice particle size distributions for this section of the cloud are shown in Figure 3.10. These represent best-fit modified gamma distributions for each of the 5-second samples of ice particles. The size distributions for the top ice layer (layer 1, red curves, not easily visible) have maxima between 200 and 300 μm, with negligible concentrations of large ($D > 500$ μm) and small ($D < 100$ μm) particles. The upper mixed-phase layer (layer 2, green curves) contains much higher concentrations of ice particles than in the lower, deeper, mixed-phase layer (layer 4, black curves), especially at the small end of the size spectrum. Keep in mind the size distributions are presented on a log-log plot. As a general rule, the lower mixed-phase layer contains more large ice particles. The high concentrations of small particles in the upper layers and relatively higher concentrations of large particles in the lower layer suggest that as these particles are growing by vapor deposition, they are also colliding and forming aggregates, which reduces the concentrations of small particles and increases the concentration of large particles. This is supported by Figure 3.10 as a significant number of size distributions in both mixed-phase layers decrease in magnitude toward the small end of the size spectrum.

The fact that there is a relatively large IWC at the top of the lower mixed-phase layer, and significant IWC content throughout the layer, may be evidence of a seeder-feeder mechanism. Based on the dew point measurements, the average relative humidity with respect to ice was 106% in the non-cloud layer between 480 mb and 540 mb. This suggests that ice particles could have "survived" the journey from the upper layers to the lower layer and triggered ice formation there. However, the layer between 480 mb and 540 mb is defined to be non-cloud because there were no ice particles or liquid droplets

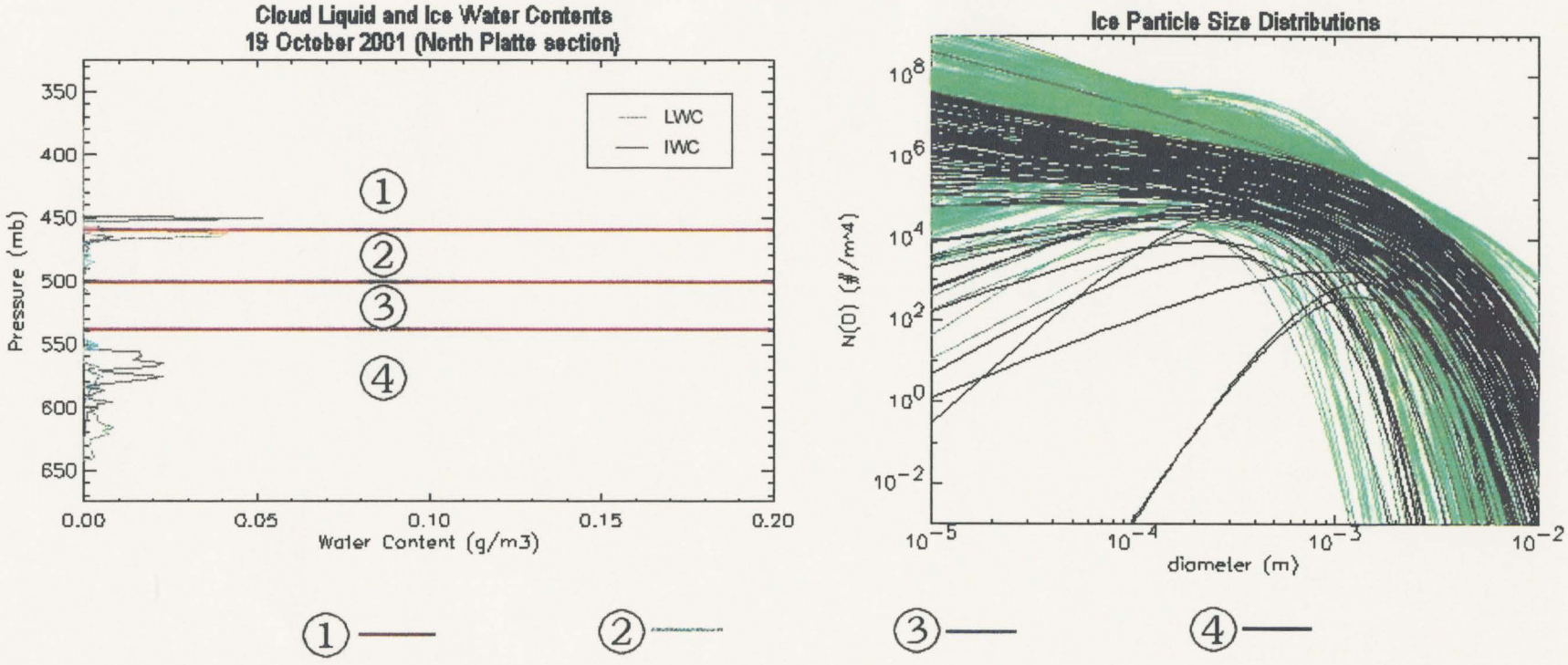

Figure 3.10. Ice particle size distributions for the North Platte section of the 19 Oct cloud, color-coded based on the numbered layer in which they were observed. Units for the size distributions are number of particles per unit volume per unit diameter.

detected in that layer. Any ice particles that did precipitate from the upper layers into the lower layer escaped detection.

Temperature, humidity and heating rate profiles for the McCook section of the 19 Oct cloud are shown in Figures 3.11 and 3.12. This section of the cloud existed at temperatures between –13 °C and –15 °C and, for all intents and purposes, was comprised entirely of liquid droplets. The horizontally averaged LWC (Figure 3.6) was less than 0.1 g m^{-3} at all heights. The radiative heating rate profiles were calculated at 1430 UTC, a half-hour after sunrise, when the cloud was rapidly dissipating. Again, the cloud was thin enough to experience solar heating throughout the cloud layer, although the latent heating was nearly a factor of two larger. Except for a very thin layer at cloud base, the cloud was experiencing a net cooling of more than 30 K day^{-1}.

The water vapor mixing ratio profiles of both sections (Figures 3.8 and 3.11) reveal that the 19 Oct cloud formed in a moist layer that existed between much drier layers above and below. With no inversions present to block upward turbulent motions, it is possible that dry air may have been entrained from below and aided the rapid dissipation of this cloud.

3.3 22 October 2001

The thickest cloud layer was observed on 22 October 2001. This cloud also contained the largest LWC and IWC values observed during CLEX-9. IR satellite images of this cloud taken during the aircraft sampling are shown in Figure 3.13. This cloud was sampled from 1401 UTC to 1613 UTC. All aircraft data from east of 102 °W longitude (east of the Nebraska panhandle) was used in this analysis, although the satellite

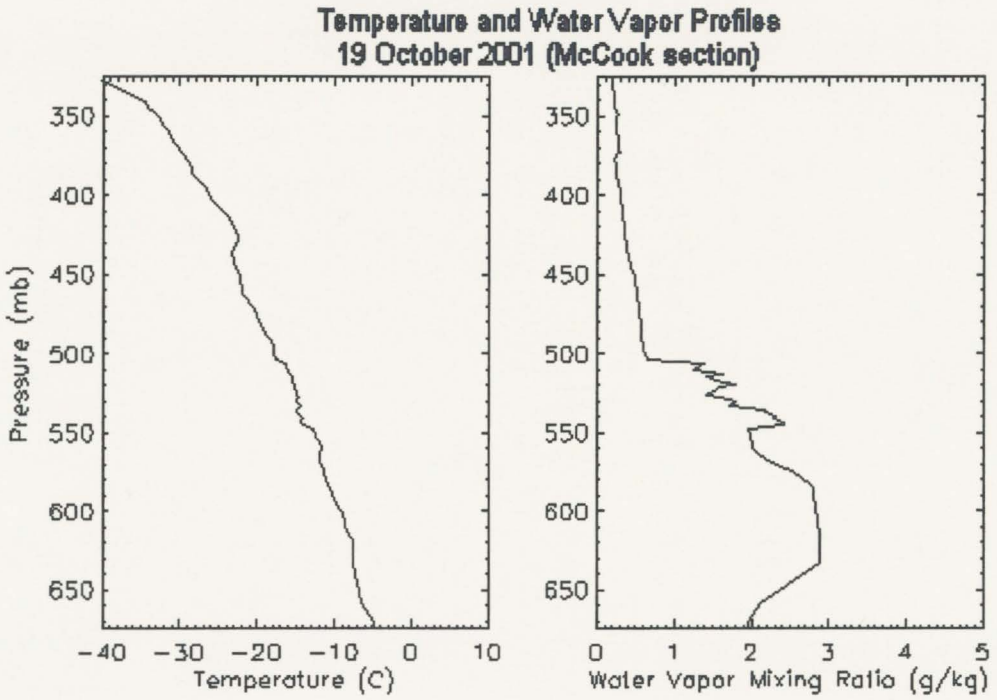

Figure 3.11. Profiles of temperature, left, and water vapor mixing ratio for the McCook section of the 19 Oct cloud. This cloud section existed between 525 and 547 mb.

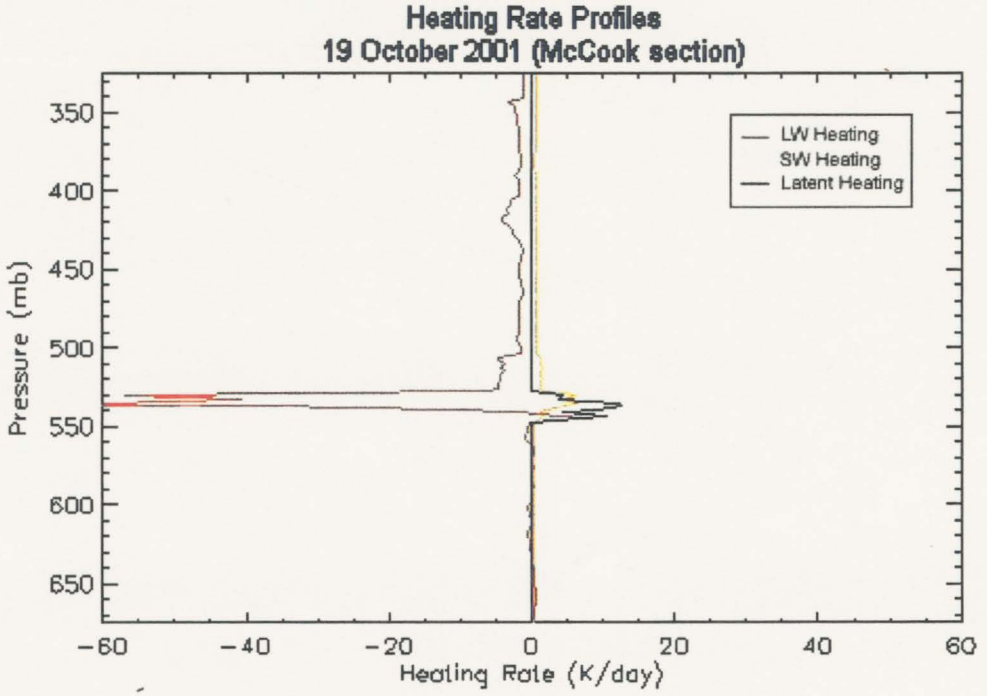

Figure 3.12. Profiles of SW, LW and latent heating rate calculated at 1430 UTC for the McCook section of the 19 Oct cloud.

imagery shows the portion of the cloud sampled was not completely filled in. Sunrise occurred at North Platte, NE at 1403 UTC.

The 22 Oct cloud existed in a very moist, deep layer (relative to the other CLEX-9 clouds) in a region of slight PVA. The general flow was from the WSW. Cloud top and cloud base were 453 mb (6.2 km MSL) and 704 mb (2.9 km MSL), respectively. Temperatures ranged from +2 °C at cloud base to –25 °C at cloud top (Figure 3.14). Profiles of LWC and IWC (Figure 3.15) show horizontally averaged LWC values as large as 0.28 g m^{-3} and horizontally averaged IWC values as large as 0.16 g m^{-3}. Note the sharp decrease in LWC with increasing pressure above 600 mb and the sharp increase in IWC below 600 mb. This is consistent with the theory that ice particles are growing at the expense of the liquid droplets due to the Wegener-Bergeron-Findeisen mechanism (Wegener 1911, Bergeron 1935, Findeisen 1938). The cloud was primarily ice between 630 and 690 mb. A small layer of liquid existed below 690 mb, where the temperatures were above 0 °C.

This distribution of liquid droplets and ice particles has a significant effect on the radiative heating rates calculated for this cloud at 16 UTC (Figure 3.16). The lower layer, comprised mostly of ice, which is not as active in the IR portion of the spectrum as liquid water, was radiatively neutral, generally emitting as much IR radiation as it absorbed. This cloud was thick enough to confine all of the solar heating in the top half of the cloud. The large LWC values in this cloud are associated with the largest latent heating rates of any of the CLEX-9 clouds. Overall, the heating rates indicate there is a strong diabatic heating (as much as 50 K day^{-1}) in the lower to middle portions of the primarily liquid layer, combined with strong diabatic cooling (greater than 60 K day^{-1}) near cloud top. As with the 14 Oct cloud, this structure of diabatic heating and cooling would result in an

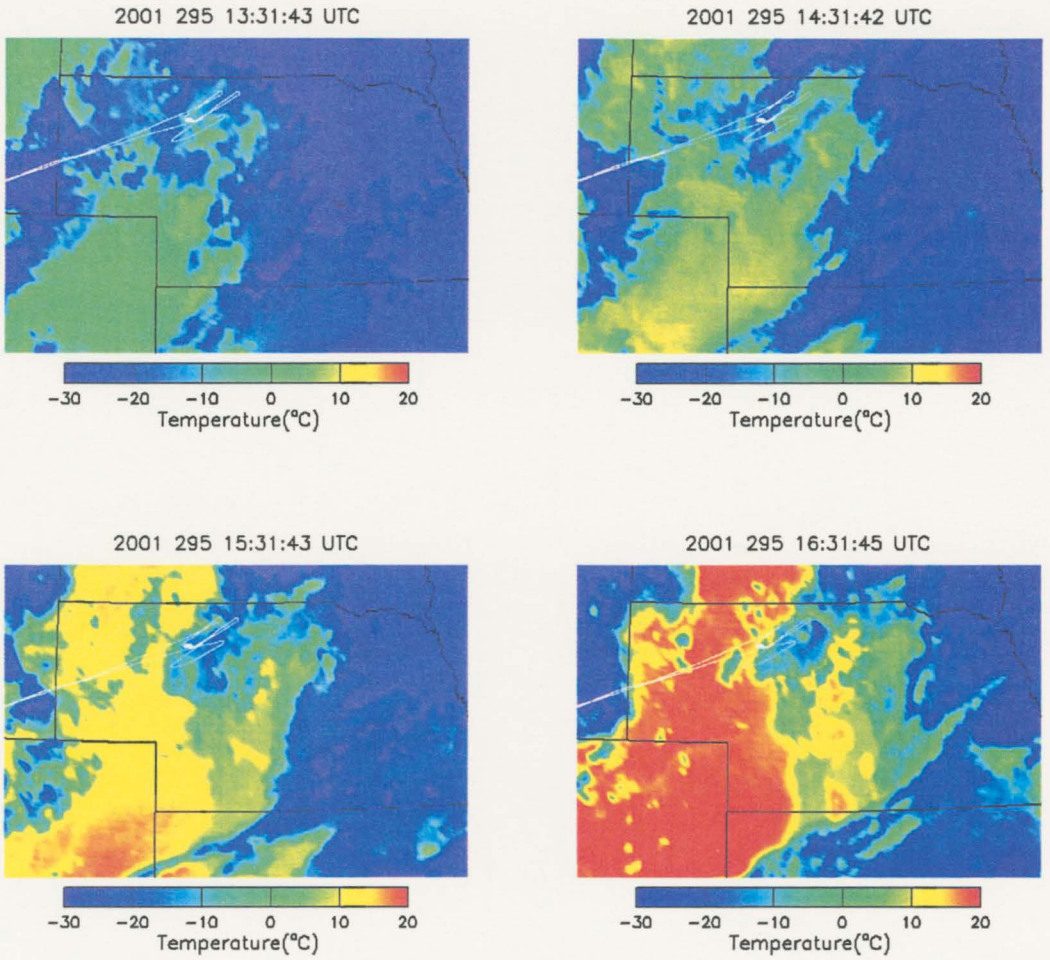

Figure 3.13. Same as Figure 3.1, except for the 22 Oct cloud.

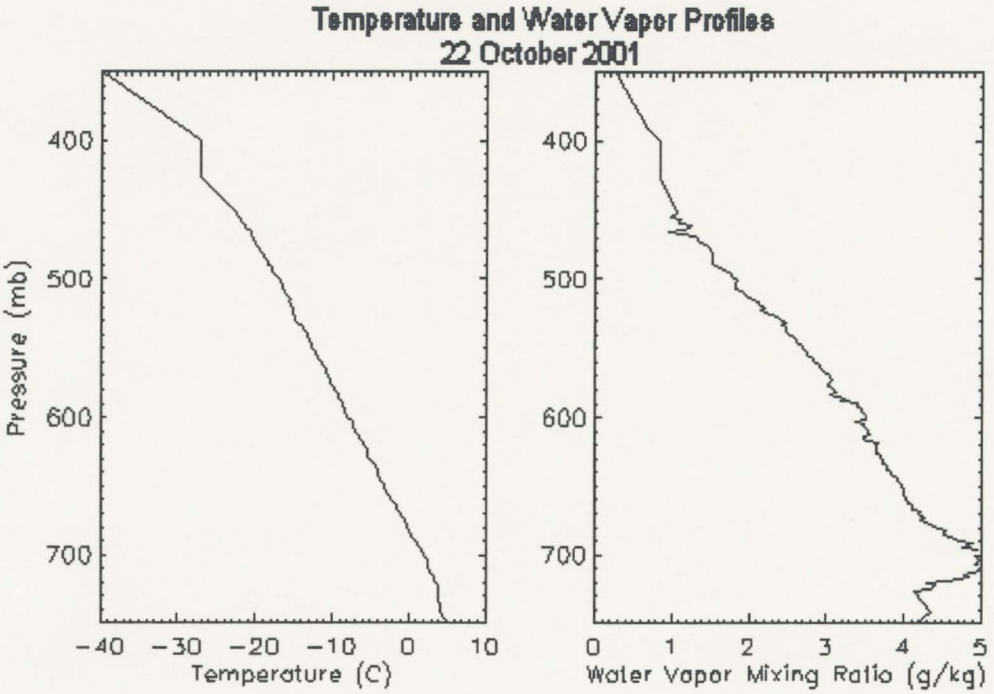

Figure 3.14. Profiles of temperature, left, and water vapor mixing ratio for the 22 Oct cloud. Cloud top and cloud base were 453 mb and 704 mb, respectively.

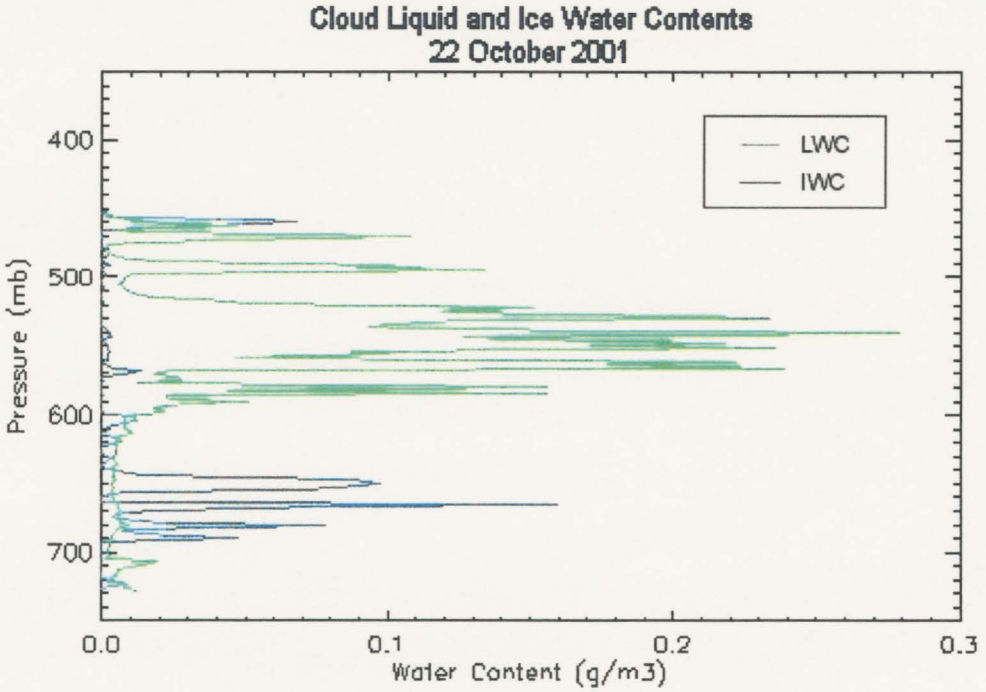

Figure 3.15. Profiles of LWC and IWC for the 22 Oct cloud.

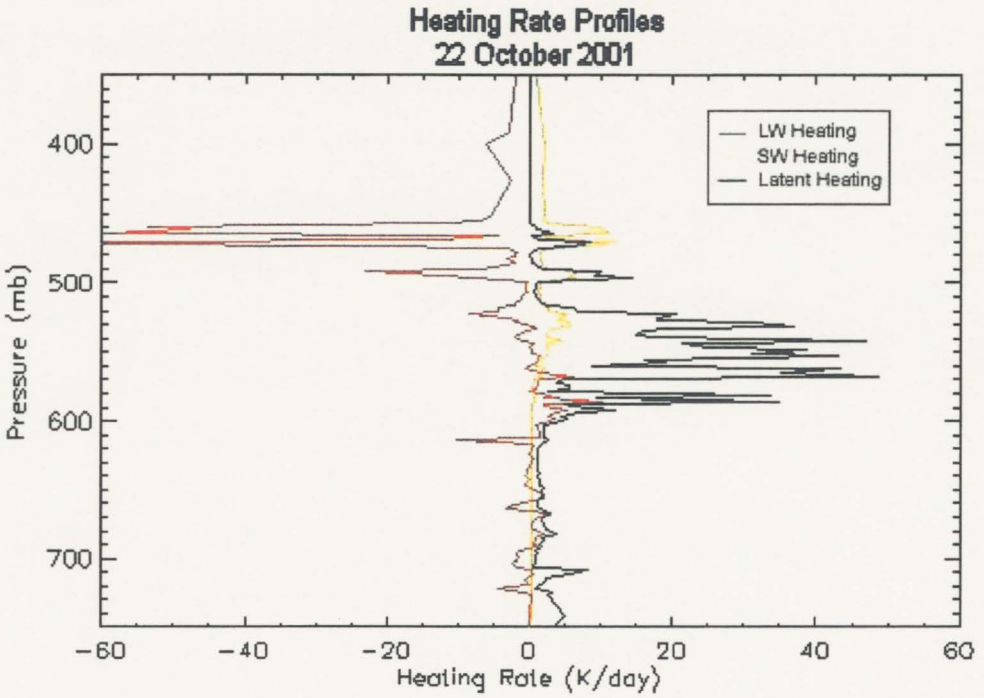

Figure 3.16. Profiles of LW, SW and latent heating calculated at 16 UTC for the 22 Oct cloud.

increase in instability in the primarily liquid layer by increasing the lapse rate. The ice layer near cloud base does not contribute to the stability or instability of the cloud, as the diabatic heating and cooling is weak and, in an average sense, does not vary much with height.

Ice particle size distributions for this cloud are shown in Figure 3.17. The variation in size distributions with height is not immediately noticeable, given the fact that the size distributions from layer 4 (near cloud base) largely overlap the distributions from layer 1 (near cloud top). At large diameters, however, it is clear that there are more large particles in layer 4 than there are in layer 1. The largest discrepancies exist between the distributions from layers 2 and 3. Layer 2 contains more large particles, and many fewer small particles than layer 3, which is lower in the cloud. This could be an indication that

layer 3 is a region of ice production. Temperatures in layer 3 varied between –8 °C and –13 °C, which includes the temperature of maximum dendritic growth (-12 °C). It is possible that ice particles formed in this layer by heterogeneous nucleation and quickly grew by vapor deposition through the Wegener-Bergeron-Findeisen mechanism and proceeded to fall into layer 4, before they could reach a size large enough to be detected by the 2D-C and 2D-P probes. This would deplete the amount of liquid water present (as mentioned above and seen in Figure 3.15) and account for the small ice water contents observed in this layer. Since no measurements of ice nuclei were made, however, this can only remain a theory.

3.4 31 October 2001

A broad expanse of mid-level cloud formed in southwest flow underneath a layer of orographically induced cirrus clouds on 31 October 2001. IR images of the cloud field (Figure 3.18) show that much of the western Great Plains was covered by cloud, which was mostly cirrus as indicated by the retrieved brightness temperatures. The mid-level cloud that formed underneath this layer of cirrus was the thinnest cloud observed during CLEX-9. This cloud field had the appearance of a set of orographic wave clouds. The main cloud layer existed between 460 mb (6.0 km MSL) and 487 mb (5.6 km MSL), with a secondary layer between 438 mb and 445 mb (6.3 to 6.4 km MSL). The cirrus cloud layer existed around 9 km MSL. Cloud top and cloud base temperatures were –17 °C and –14 °C, respectively (Figure 3.19). Horizontally averaged LWC values were less than 0.1 g m^{-3} and peaked at the same height as the horizontally averaged IWC (Figure 3.20).

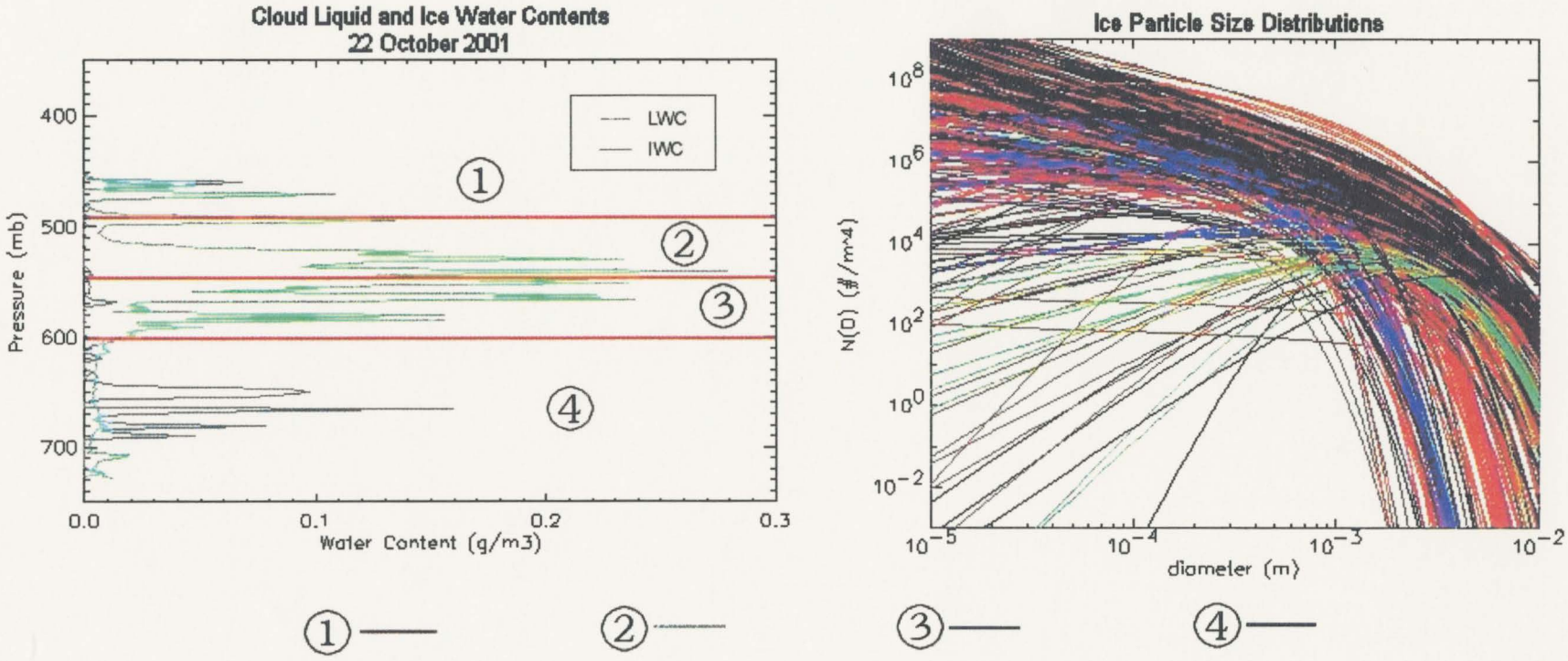

Figure 3.17. Same as Figure 3.10, except for the 22 Oct cloud.

Radiative and latent heating rate profiles taken at 15 UTC (Figure 3.21) reveal moderate net diabatic heating near cloud base and moderate net diabatic cooling near cloud top. Sunrise at North Platte, NE occurred at 1414 UTC, and with the low sun angle, the SW heating was small near cloud top. It should be noted that, since no direct measurements were made inside the over-running cirrus layer, the heating rate profiles neglect the effects of the cirrus cloud. Addition of the cirrus cloud into the radiative transfer calculations would decrease both the SW heating and LW cooling at the top of the mid-level cloud, since the cirrus would absorb some of the solar radiation and would also emit LW radiation downward that would be absorbed by the mid-level cloud. The amount of solar radiation absorbed by the cirrus layer, would be small however, since ice particles are more effective scatterers of solar radiation than absorbers. The increase in LW radiation absorbed by the top of the mid-level cloud due to emission from the cirrus layer would decrease the LW cooling at cloud top, which would decrease the instability produced by the diabatic heating profile shown in Figure 3.21.

Ice particle size distributions (Figure 3.22) show that, overall, this cloud contained relatively few large particles and many small particles. Figure 3.22 also shows that there is very little change with height in the shape of the distributions. Since this cloud was the thinnest of the CLEX-9 clouds, ice particles would have the least amount of cloud depth, and hence time, over which to grow by vapor deposition and aggregation. They would not be very big by the time they fell out of the bottom of the cloud and began evaporating.

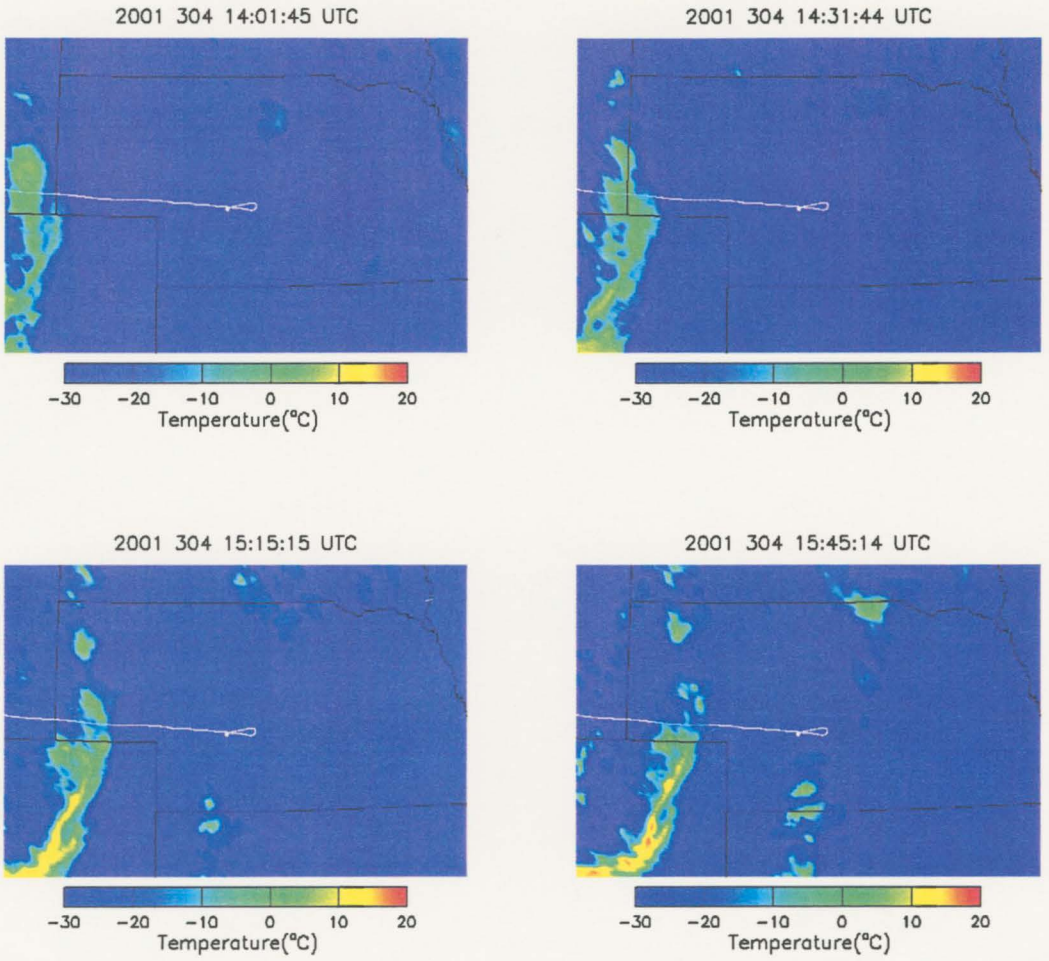

Figure 3.18. IR satellite images of the 31 Oct cloud field taken at roughly half-hour intervals during the UWKA sampling. The flight path of the UWKA is also shown. Most of what is visible in these images is the overlaying cirrus deck. Also noticeable is the advancing dry slot (i.e. the region of relatively high brightness temperatures).

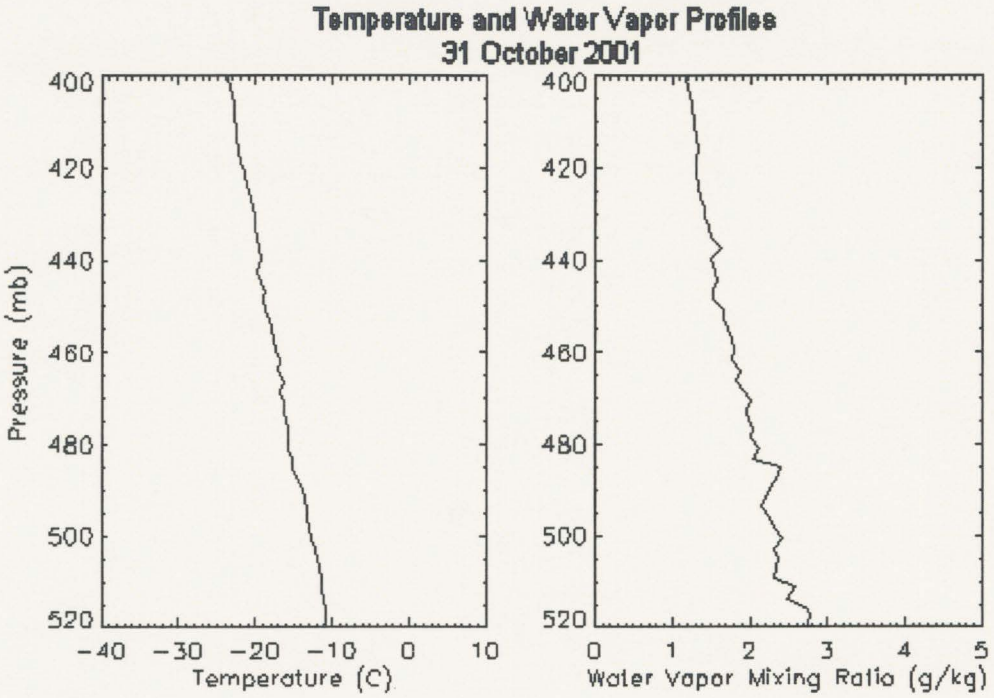

Figure 3.19. Profiles of temperature, left, and water vapor mixing ratio for the 31 Oct cloud.

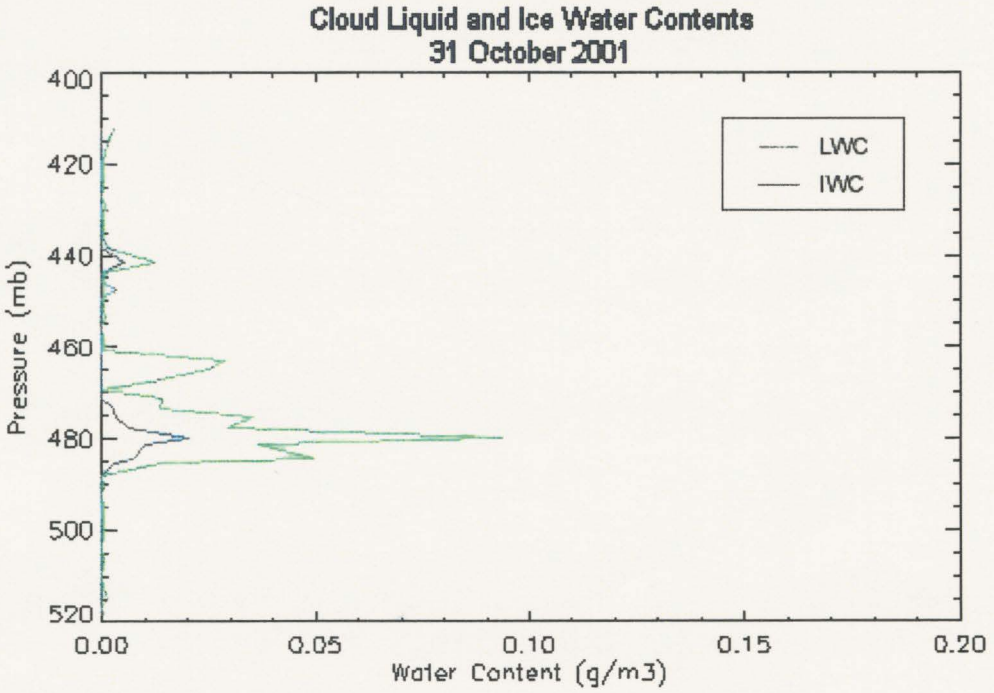

Figure 3.20. Profiles of cloud liquid and ice water content for the 31 Oct cloud.

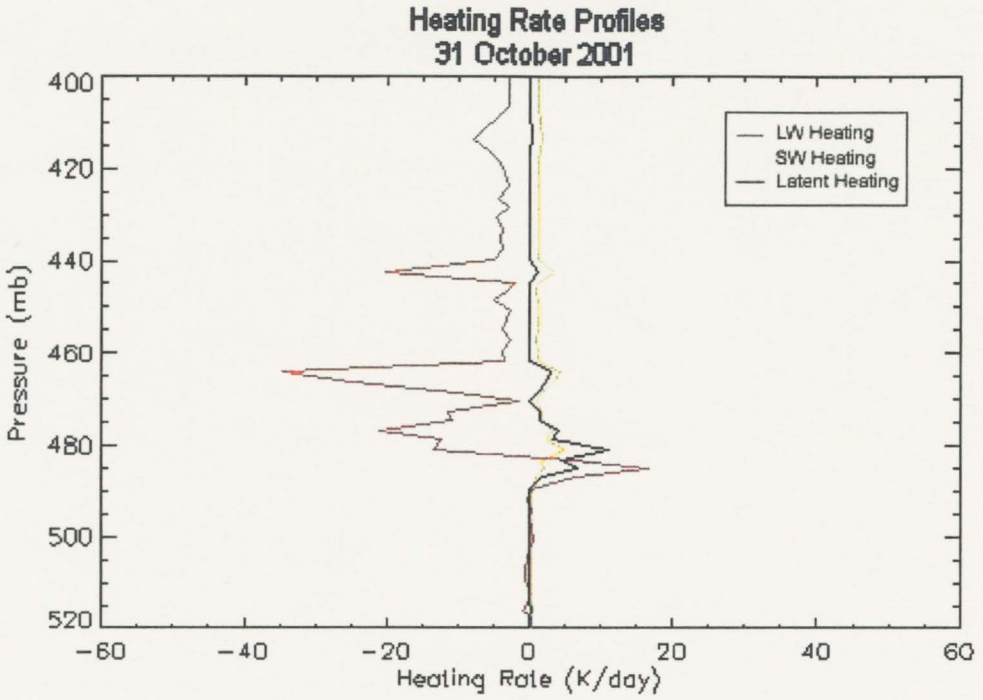

Figure 3.21. Profiles of LW, SW and latent heating rate at 15 UTC for the 31 Oct cloud.

3.5 2 November 2001

The final cloud sampled during CLEX-9 formed during the overnight hours in northwest flow in a region of PVA on 2 November 2001. This cloud was isolated from other clouds and sustained itself through the night. After sunrise, however, the cloud began to dissipate and was gone three hours later. IR satellite images (Figure 3.23) show this nicely. Sunrise was 1416 UTC at North Platte, NE. This cloud serves as an example of how solar radiation may shorten the lifetimes of mid-level clouds.

The 2 Nov cloud was approximately 550 m thick and had cloud top and base pressures (heights) of 558 mb (4.7 km MSL) and 600 mb (4.1 km MSL). The maximum horizontally averaged LWC value of 0.14 g m^{-3} occurred in the middle of the cloud layer

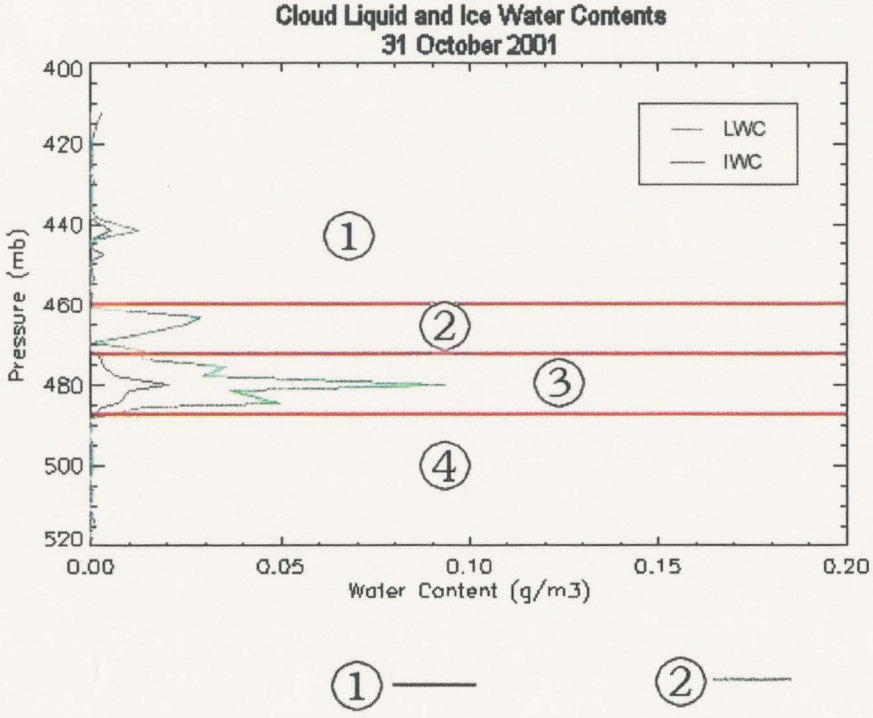

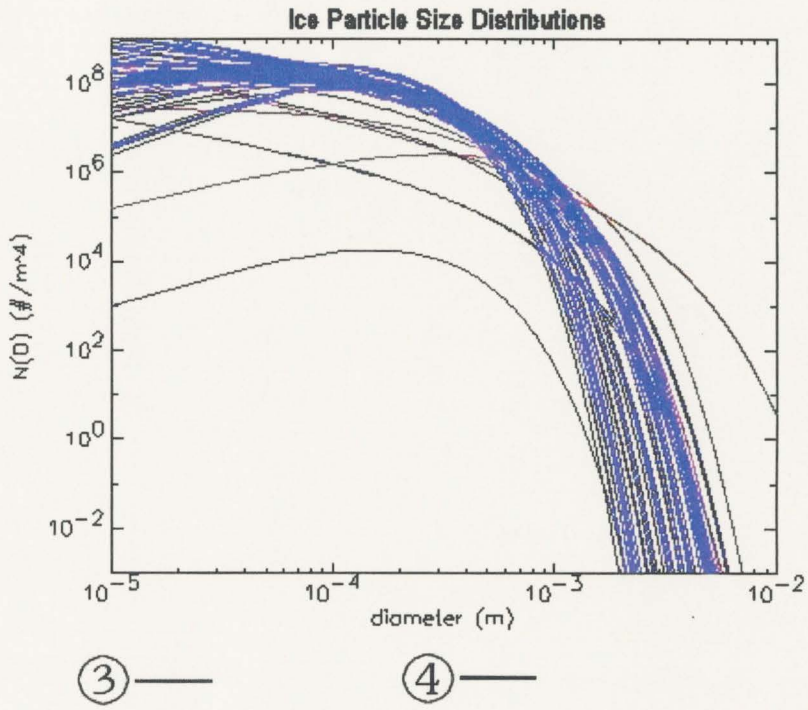

Figure 3.22. Same as Figure 3.17, except for the 31 Oct cloud.

(Figure 3.24), suggesting that entrainment at cloud top may have been important in this cloud. A shallow layer of ice existed near cloud base with small horizontally averaged IWC values (>0.01 g m^{-3}). It is suggested that the Wegener-Bergeron-Findeisen mechanism was active here, as peak IWC values occurred at the same height as the greatest change in LWC with height occurred. Although the ice particles were able to reach precipitation size within this layer (i.e. the cloud averaged ice effective radius was 683 μm), particle concentrations were typically 1-2 orders of magnitude less than in the 19 Oct and 22 Oct clouds, which explains the small IWC values observed.

Aggregation was a significant contributor to the low concentrations of ice particles. The effects of aggregation can be seen in the ice particle size distributions (Figure 3.25). A large fraction of the size distributions have maxima between 200 and 2000 μm, with much lower concentrations of particles smaller than 100 μm in diameter. Temperatures in the cloud where most of the ice was found were between –11 °C and –13 °C (Figure 3.26). This coincides with the temperature of maximum dendritic growth rate (-12 °C). Dew point measurements reveal the relative humidity with respect to ice in this layer was near 112%. The presence of dendrites and relatively high ice supersaturations are the factors that Ohtake (1970) determined were necessary for the "interlocking mechanism" to occur, whereby the arms of colliding dendrites would interlock and cause the particles to stick together. This is the likely method of aggregation in this cloud.

Heating rate profiles taken at 16 UTC (Figure 3.27) show the typical LW heating at cloud base and LW cooling at cloud top. SW heating at cloud top was similar in magnitude to the LW heating at cloud base. This cloud contained enough liquid water to constrain the SW heating to the top half of the cloud and have relatively large latent heating rates (up to 39 K day^{-1}) throughout the cloud. Overall, there was a net heating of

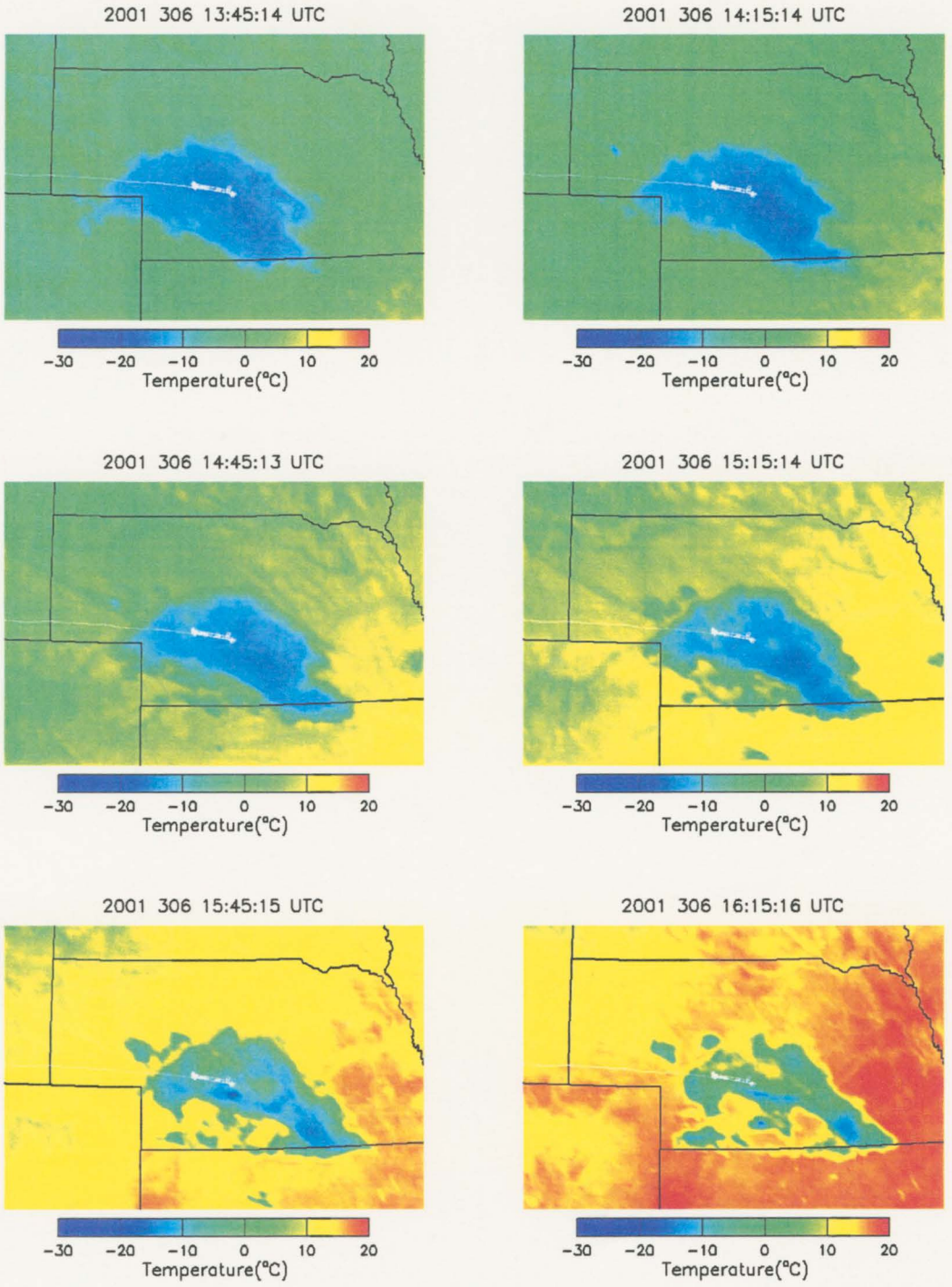

Figure 3.23. IR satellite images taken every half-hour during the UWKA flight on 2 Nov. The aircraft flight path is also shown. Note the drastic change in appearance of the cloud after sunrise.

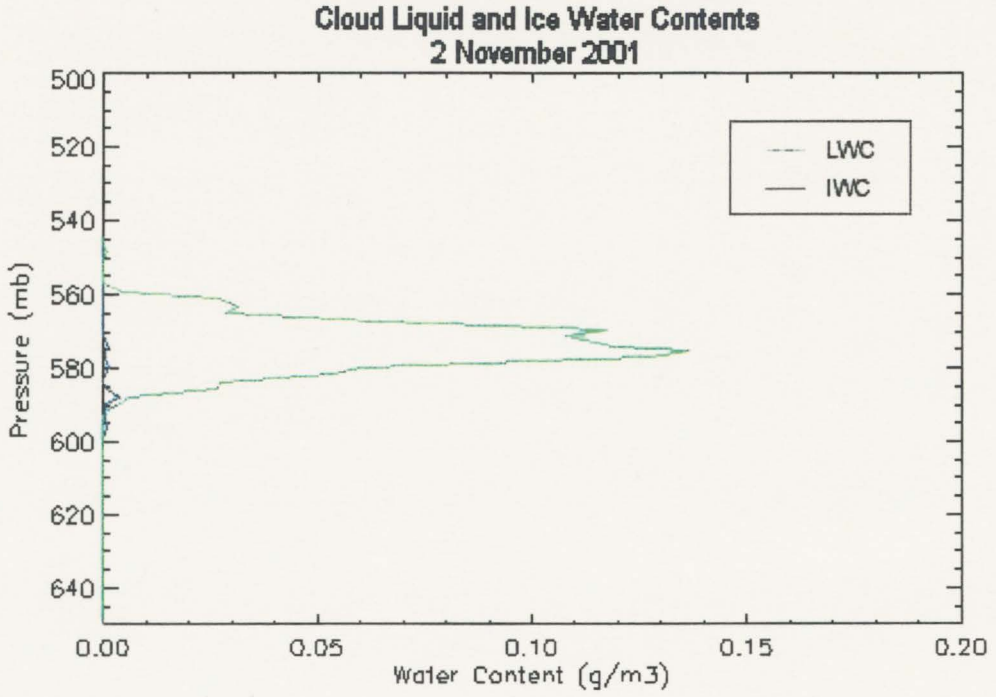

Figure 3.24. Profiles of cloud liquid and ice water contents for the 2 Nov cloud.

up to 46 K day^{-1} near cloud base and a net cooling of up to –29 K day^{-1} near cloud top. Before sunrise, the lack of SW heating would lead to a net cooling near cloud top of near –40 K day^{-1}. Again, we see that the presence of SW heating after sunrise reduces the cloud top cooling, which reduces the instability that the net heating rate profile promotes. Radiation played an important role in the morphology of this cloud.

3.6 Overview of Cloud Properties

The previous sections detailed the observations made of five mid-level clouds that were sampled during CLEX-9. In this section, we combine all of these observations to compare and contrast these clouds with each other, and with the mid-level clouds that

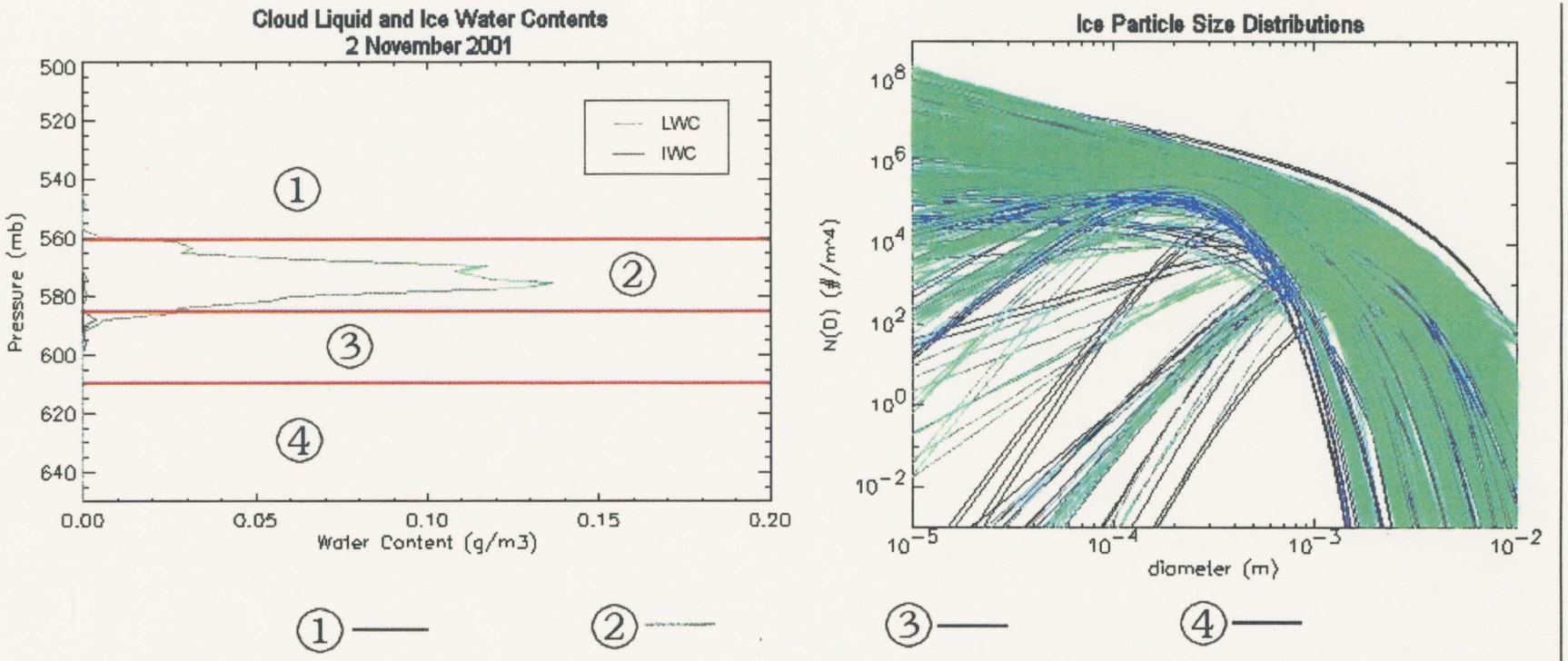

Figure 3.25. Same as Figure 3.22, except for the 2 Nov cloud.

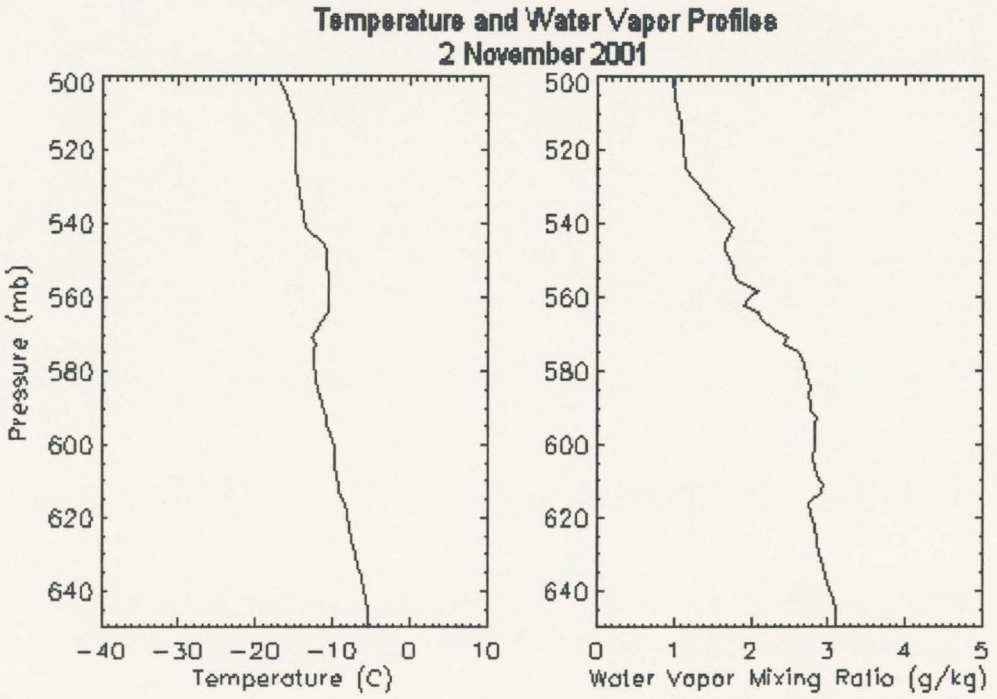

Figure 3.26. Profiles of temperature, left, and water vapor mixing ratio for the 2 Nov cloud.

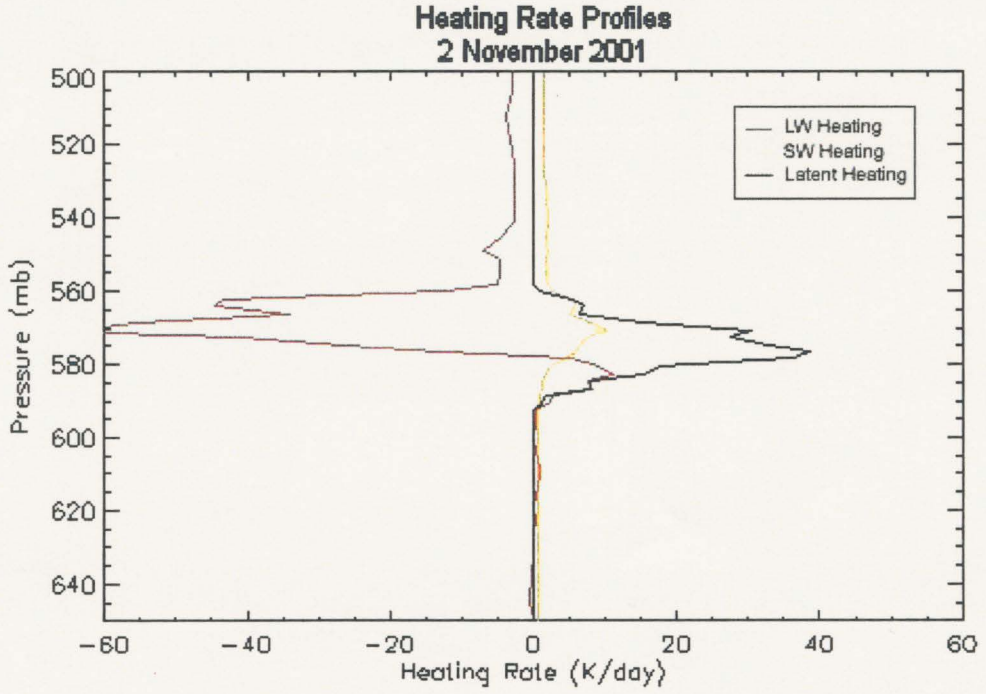

Figure 3.27. Profiles of LW, SW and latent heating rate at 16 UTC for the 2 Nov cloud.

have been observed in previous studies. Also presented here are the derived properties that are useful in remote sensing and modeling studies of mid-level clouds. Making claims of universal truths about mid-level clouds based on these five clouds is hazardous. Most aircraft studies to date exploring the properties of mid-level clouds include the results of six or fewer clouds. If we include the results of Heymsfield et al. (1991), Tulich and Vonder Haar (1998) and Fleishauer et al. (2002), the total number of similar mid-level clouds is fifteen. There are some patterns that begin to emerge when we compare and contrast this set of clouds.

Let us first review the results of CLEX-9 that were presented in previous sections of this chapter. The five clouds sampled had depths of between 250 m and 3100 m. Three of the five clouds were less than 1 km thick. Cloud bases were between 2.9 km and 5.6 km MSL. Temperatures ranged from +2 °C to –25 °C in cloud. Two of the clouds (14 Oct and 19 Oct-McCook section) were, for all intents and purposes, comprised of liquid only. The remaining clouds were mixed-phase. The North Platte section of the 19 Oct cloud was the only multi-layered cloud sampled, and contained the largest ratio of IWC to LWC. Maximum LWC values observed were between 0.27 g m^{-3} and 0.94 g m^{-3}, with maximum horizontally averaged values between 0.04 g m^{-3} and 0.28 g m^{-3}. Maximum IWC values for the mixed-phase clouds derived using the methods of section 2.3 ranged from 0.05 g m^{-3} to 0.50 g m^{-3}, with horizontally averaged IWC maxima from < 0.01 g m^{-3} to 0.16 g m^{-3}.

Heating rate profiles in all but the North Platte section of the 19 Oct cloud revealed net diabatic heating near cloud base and net diabatic cooling near cloud top, largely due to IR radiation. Heating at cloud base and cooling at cloud top leads to an increase in the lapse rate, which increases the instability within the cloud layer. The North Platte section of the 19 Oct cloud, in contrast, experienced net cooling throughout both of the cloud layers, which is presumably due to the fact that this cloud contained the smallest ratio of

LWC to IWC, and liquid droplets are more active radiatively than ice particles are. Also contributing to the net cooling throughout this cloud was an absence of solar heating due to the fact that this cloud was sampled before sunrise. The presence of solar radiation after sunrise decreased the cloud top cooling by more than 10 K day^{-1} in some cases, depending on the solar zenith angle and microphysical composition. This reduces the instability within the cloud layer produced by the net heating profile. The importance of radiation on the lifetime of these clouds will be discussed in more detail in the next chapter.

The values of LWC, temperature and cloud depth compare well with previous studies of mid-level clouds. Table 3.1 shows the values observed during CLEX-9 along with those from CLEX-5 (Fleishauer et al. 2002), CLEX-1 (Tulich and Vonder Haar 1998) and FIRE (Heymsfield et al. 1991). These studies all featured mid-level clouds in continental North American environments. Also shown in Table 3.1 are the results of Hobbs and Rangno (1985, 1998), Pinto (1998) and Paltridge et al. (1986). Hobbs and Rangno (1985, 1998) and Pinto (1998) observed mid-level and mixed-phase clouds in marine and Arctic environments. Paltridge et al. (1986) observed a mid-level, mixed-phase cloud over Australia. For the most part, mid-level clouds that have been observed were less than 1 km thick, with average LWC values less than 0.5 g m^{-3} and temperatures ranging from near freezing to between –20 °C and –30 °C.

Of particular interest here is how the clouds observed during CLEX-9 compare with the clouds of previous CLEX studies and the clouds of Heymsfield et al. (1991). These studies were performed on continental clouds over the Great Plains and Midwest of the United States and include observations of fifteen mid-level clouds. Of the fifteen clouds, four were comprised of liquid only (or had negligible amounts of ice present), one was comprised of ice only and ten were mixed-phase. Four of the clouds were multi-layered systems. The coldest clouds were the two observed by Heymsfield et al. (1991).

Table 3.1. Cloud depth, liquid water content (LWC), and temperature (T) comparison between this study (CLEX-9) and other observational studies of mid-level, mixed-phase clouds. CLEX-9 values generally fall within the range of all other measurements.

Field Study	*Cloud Depth* [m]	*LWC* [g m^{-3}]	*T* [°C]
Continental North American			
CLEX-9	**250-3100**	**.04 - .28**	**+2 to -25**
CLEX-1	**200-800**	**.03 - .31**	**-10 to -23**
CLEX-5	**500-2300**	**.005 - .35**	**-1 to -31**
Heymsfield et al. (1991)	**200-500**	**.01 - .12**	**-29 to -31**
Marine and Arctic			
Hobbs and Rangno (1985)	**100-1000**	**< .1 – 1.3**	**-4.5 to -26**
Hobbs and Rangno (1998)	**30-800**	**.02 - .14**	**-1 to -31**
Pinto (1998)	**130-290**	**.005 - .1**	**-13 to -20**
Continental Australian			
Paltridge et al. (1986)	**300-700**	**.01 - 1.2**	**-6 to -11**

These clouds also had the highest bases (>7 km MSL). It is interesting to note that one of these mid-level clouds was liquid-only, while one was mixed-phase. Both existed underneath layers of cirrus cloud at similar temperatures. The liquid-only cloud was further from the cirrus, so it is possible that the seeder-feeder mechanism was not active in this case. It is also possible that ice particles that formed were too small to be detected. The liquid-only cloud was very thin (~200 m thick) and ice particles would likely not have grown to an appreciable size before they exited the base of the cloud and

began to evaporate. The liquid-only clouds of this study and CLEX-5 were ~400 and ~600 m thick. The McCook section of the Oct 19 cloud was liquid-only as well, and was ~250 m thick. Temperatures in these clouds were greatly varied (-6 °C to –22 °C). Heymsfield and Miloshevich (1993) found that homogenous nucleation would only create measurable ice particles in temperatures less than –35 °C. These liquid-only clouds are therefore too warm for homogeneous nucleation and heterogeneous nucleation must not be very active either, since no (or very few) ice particles were observed. This signifies a lack of ice nuclei. We then speculate that the mixed-phase clouds contained sufficient amounts of ice nuclei, since temperatures were never observed below –35 °C in any of these clouds. No ice nuclei measurements were made in any of these studies to verify this, however.

The single-layered mixed-phase clouds in this study and those of CLEX-5 and Heymsfield et al. (1991) all had the largest observed values of IWC near cloud base. This suggests that the ice particles that form grow by vapor deposition from the Wegener-Bergeron-Findeisen mechanism and/or by aggregation and fall through the cloud. They continue to grow as they fall due to these processes and reach their maximum size near cloud base, before they exit the cloud and begin sublimating. This, combined with the fact that these clouds formed at different temperatures, explains why ice water contents have been found to be poorly correlated with temperature (e.g. Hobbs and Rangno 1998, Fleishauer et al. 2002).

The multi-layered cloud system of this study compares well with those of Fleishauer et al. (2002). They generally exhibit a more uniform profile of IWC with height than in the single-layer clouds. This is most likely explained by seeder-feeder mechanisms that occur between the various layers. Ice particles that form in the upper layers fall through the cloud-free layers and initiate ice production in the lower layers. This leads to a significant IWC being measured at the tops of these layers. Fleishauer et al. (2002)

presents more evidence in support of this theory. However, ice particle concentrations observed in the cloud-free layers are quite low, and may be too low to explain the observed ice particle concentrations at the tops of the various layers. The multi-layered cloud system observed by Tulich and Vonder Haar (1998) during CLEX-1 was unusual in that it did not contain significant amounts of ice. It is this author's opinion that a lack of ice nuclei existed. Temperatures in this cloud were above the limit for homogeneous nucleation presented in Heymsfield and Miloshevich (1993).

We now turn our attention to the cloud properties that are useful for remote sensing and modeling purposes. Table 3.2 shows the values of cloud depth, liquid water path (LWP), ice water path (IWP), domain-averaged LWC and IWC, domain-averaged liquid and ice effective radii and optical thickness for each of the clouds presented in this study. For comparative purposes, similar results from Fleishauer (2001) are shown in Table 3.3. Cloud depth and the liquid and ice effective radii were calculated as mentioned previously (see sections 2.2, 2.3 and 3.1). The LWP and IWP are defined by

$$\begin{aligned} LWP &= \int (LWC)dz \\ IWP &= \int (IWC)dz \end{aligned} \tag{3.1}$$

where z is height. For this study, the LWP and IWP were calculated by converting the profiles of LWC and IWC into 30 m averages in the vertical and setting dz = 30 m. This was done for consistency with Fleishauer (2001). As long as the cloud droplets and particles are much larger than the wavelength of the radiation (i.e., in the solar and near-IR portion of the spectrum), it can be shown that the optical thickness due to liquid and ice are (Stephens 1994)

Table 3.2. List of cloud radiative parameters useful for remote sensing and modeling purposes, including cloud depth, domain-averaged LWC and IWC, liquid water path (LWP) and ice water path (IWP), domain averaged liquid and ice effective radii ($r_{e,l}$ and $r_{e,i}$, respectively) and optical depth, τ, for each of the clouds presented in this study.

Date	Cloud Depth (m)	$\overline{LWC}$ (g m^{-3})	LWP (g m^{-2})	$r_{e,l}$ (μm)	$\overline{IWC}$ (g m^{-3})	IWP (g m^{-2})	$r_{e,i}$ (μm)	τ
14 Oct 01	458	0.038	22.3	10.9	0	0	------	5.4
19 Oct 01 North Platte	1691*	0.004	5.7	11.0	0.005	9.1	624.4	0.8
19 Oct 01 McCook	248	0.052	16.0	7.5	0	0	------	3.2
22 Oct 01	3106	0.049	156.9	9.5	0.010	32.4	1163.7	24.8
31 Oct 01	409	0.026	14.1	9.9	0.004	2.1	267.7	2.2
2 Nov 01	544	0.044	28.0	6.2	0.001	0.3	682.7	6.8

* Cloud depth for the North Platte section of the 19 Oct cloud is the sum of the depths of the individual layers and does not include the depth of the non-cloud layer.

Table 3.3. Same as Table 3.2, except taken from the results of Fleishauer (2001).

Date	Cloud Depth (m)	$\overline{LWC}$ (g m^{-3})	LWP (g m^{-2})	$r_{e,l}$ (μm)	$\overline{IWC}$ (g m^{-3})	IWP (g m^{-2})	$r_{e,i}$ (μm)	τ
11 Nov 99	525	0.13	84.6	12.2	0.02	8.5	114.3	10.5
2 Dec 99	550	0.06	27.2	7.8	0.01	2.1	146.9	5.2
5 Dec 99	610	0.09	73.4	10.2	0	0	-----	10.8
10 Mar 00	1825*	0.01	19.9	14.0	0.01	32.4	212.9	10.9
12 Apr 00	2360*	0.10	167.4	21.4	0.23	727.9	314.9	15.6

* The 10 Mar and 12 Apr cases were multi-layered cloud systems. Cloud depth is again the sum of the depths of the individual layers and does not include the depths of non-cloud layers.

$$\tau_l = \frac{3(LWP)}{2\rho_l r_{e,l}}$$
$$\tau_i = \frac{3(IWP)}{2\rho_i r_{e,i}} \qquad (3.2)$$

where ρ_l = 1.0 g cm^{-3} is the density of liquid water, ρ_i = 0.9 g cm^{-3} is the density of ice and $r_{e,l}$ and $r_{e,i}$ are the cloud-averaged effective radii of liquid droplets and ice particles given by (2.3) and (2.6), respectively. The total optical thickness, τ, presented in Tables 3.2 and 3.3 is the sum of the individual optical thicknesses given by (3.2).

Comparing Tables 3.2 and 3.3, we see that the clouds of this study were generally thinner in a cloud depth sense compared with those of Fleishauer (2001). This leads to generally lower liquid water paths and optical depths, since the liquid water dominates the total optical depth. The liquid droplet effective radii compare rather well, and for the most part, are near 10 μm. The average ice water contents, however, are a factor of 2-10 less in this study. This is due to the fact that Fleishauer (2001) used the raw data from a 2D-C probe and made no effort to account for non-sphericity of the particles. As mentioned previously, this leads to an overestimation of particle volume by a factor of 5-20, depending on particle habit, which leads to an overestimation of IWC. The ice water paths are similar, though. The ice particle effective radii give further support to the idea that as particles grow by the Wegener-Bergeron-Findeisen mechanism and by aggregation, they reach their maximum size near cloud base. This is seen in the values of $r_{e,i}$, which increase with increasing cloud depth. The deeper the cloud layer, the more time an ice particle of a given size will remain in the cloud where it can grow by these processes. Liquid droplet effective radii are not as well correlated with cloud depth. It might be expected that the liquid droplet effective radius would be negatively correlated with IWC, since the Wegener-Bergeron-Findeisen mechanism would deplete the liquid

droplets of their water molecules. Tables 3.2 and 3.3 show that this is not the case and, if anything, $r_{e,l}$ is positively correlated with IWC. The liquid droplet effective radius is not well correlated with water vapor mixing ratio. The explanation of why $r_{e,l}$ is the way it is remains unknown.

4. The Importance of Radiation in the Lifetimes of Mid-level Clouds

In the previous chapter, we presented observations of five mid-level clouds and compared them with previous observations made of continental North American mid-level clouds. In this chapter, we discuss the microphysical and dynamical processes inherent in the formation, sustenance, and dissipation of mid-level, mixed-phase clouds in general as well as in the five clouds of this study in particular. It was mentioned previously the role that radiation plays in maintaining mid-level clouds by increasing the lapse rate within the cloud layer. But how important is radiation in the lifetime of mid-level clouds? To answer that question, a simple model was developed to determine the relative importance of the main processes that affect cloud lifetime, namely subsidence, entrainment, radiation and precipitation. This model and its results are presented in section 4.2. In the next section, we outline these processes and how they effect cloud lifetime.

4.1 Processes that Effect the Lifetime of Mid-level Clouds

It was mentioned in the introduction that mid-level clouds are, for the most part, transient. This is due to the complex interactions between the clouds and their

environment, as well as the complex interactions between their constituent particles. The liquid droplets and ice particles (when present) are in a constant struggle with each other over the available water vapor molecules. Cloud parcels, as we shall see, not only must overcome this inner turmoil, but must also defend themselves from subsidence and the entrainment of outside air.

The two ingredients necessary for the formation of any cloud are moisture and lift. Assuming a typical tropospheric temperature sounding, air parcels with some water vapor pressure, when lifted, enter layers of the atmosphere with lower temperatures, and hence lower saturation vapor pressures. When the parcels reach a height where the temperature of the ambient atmosphere is equal to (or below) the dew point of the lifted parcels, saturation (or supersaturation) occurs and water vapor molecules will begin to condense onto cloud condensation nuclei (CCN) that are present and form liquid droplets. If there are ice nuclei present, and the temperatures are below 0 ^{o}C, the vapor molecules may deposit directly into the ice phase. Ice nuclei may also convert liquid droplets into ice particles through immersion freezing or contact nucleation. The supply of water vapor is critical for the formation and sustenance of mid-level clouds (Rauber and Tokay 1991, Korolev and Isaac 2003). Since, by definition, mid-level clouds form above the boundary layer, this water vapor cannot come directly from the surface, but only from elevated layers of moisture due to the remnants of other clouds that existed in the mid-troposphere or that were transported by favorable dynamics that carried moisture out of the boundary layer and into the mid-troposphere. The lift may come from convection, gravity waves, mountain waves, frontal boundaries or the passage of potential vorticity anomalies.

For CLEX-9, the target clouds were non-orographic, non-frontal and not associated with convection. The 31 Oct cloud, however, was orographically produced. The remaining four clouds were true to the intended form and were not associated with

frontal boundaries, deep convection or orography. Those clouds all formed in areas of positive vorticity advection (PVA), which is an area of lift (Hoskins et al. 1985). This is due to the fact that potential vorticity is conserved for adiabatic, frictionless flow. Potential vorticity is a measure of the ratio of the absolute vorticity to the depth of the fluid. In positive potential vorticity anomalies, the vorticity increase leads to an increase in the depth of the column, and therefore isentropes bow upward. As air parcels, which move along isentropic surfaces, enter a positive potential vorticity anomaly (a region of PVA), they are lifted. As air parcels exit the anomaly (a region of negative vorticity advection, or NVA), they descend back to (roughly) their original height. The rear of the vorticity anomaly is therefore a region of sinking air, or subsidence. So as the vorticity anomaly moves past, the air parcels that comprise the cloud experience a period of lift followed by a period of subsidence. The presence of PVA and mid-level moisture were the main factors used to forecast the occurrence of mid-level clouds during the field experiment. As shown in the next section, the passage of potential vorticity anomalies may explain the relatively short lifetimes of mid-level clouds. This may also explain the relatively weak updrafts observed.

The simple picture presented above is complicated by radiation, entrainment and precipitation. The presence of liquid water and ice particles modifies the radiative heating and/or cooling within the cloud layer as the cloud particles absorb and emit radiation to a greater extent than the ambient gases and aerosols. This results in a net radiative heating at the base of the cloud layer and a net radiative cooling at the top of the cloud layer as shown in Chapter 3. The lapse rate is therefore increased in the cloud layer, which increases the instability and, hence, the lift. This alone acts to increase the lifetime of the cloud, but radiation may also act to decrease the lifetime of the cloud indirectly. If the upward motion produced by the radiative heating profile and dynamic lift is large enough, the cloud parcels may be detrained into the overlying layer of drier air

and evaporate (Cotton and Anthes 1989). Also, the radiative cooling at cloud top is a primary cause of entrainment (Heymsfield et al. 1991). Since cooler air at the same pressure is denser, the radiative cooling causes air parcels at cloud top to sink, which promotes the entrainment of drier air aloft into the cloud. Convective processes can mix the cloud right out of existence. Detrainment was not a significant factor in any of the CLEX-9 clouds, as vertical velocities were rather weak and vigorous convection was not present. Entrainment will be explored more in the next section.

Microphysical processes have their part in the morphology of mid-level clouds as well, especially when ice is present. Ice particles grow at the expense of the liquid droplets - the so-called Wegener-Bergeron-Findeisen mechanism – due to the fact that the saturation vapor pressure over an ice surface is less than that over a liquid surface. In an anthropomorphic line of thought, the ice particles, wanting to see fewer water vapor molecules in their surroundings, attract the vapor molecules and lower the vapor pressure. If there is not enough vapor present to satisfy the liquid droplets and ice particles, the liquid droplets will sacrifice their water molecules, since they prefer a higher vapor pressure. The droplets will then evaporate as the ice particles grow. As the ice particles grow, so do their terminal velocities and so the particles will fall through the cloud, exit through cloud base and take their water molecules with them. The early work by Bergeron (1933) and Findeisen (1938) showed that this process leads to an unstable situation in mixed-phase clouds if the ambient vertical velocity is zero. More recent work by Korolev and Isaac (2003) showed that a uniform vertical velocity is also unstable. The presence of ice will reduce the lifetime of the cloud. When all the liquid is gone, the cloud has "glaciated", which usually leads to rapid dissipation. Glaciation time is highly dependent on ice particle concentrations (Korolev and Isaac 2003, Harrington et al. 1999) since more ice particles can attract more vapor molecules and deplete the liquid droplets faster. The longevity of mixed-phase clouds in a microphysical sense depends

on a combination of one or more of the following: low concentrations of ice particles or ice nuclei (Pinto 1998), supersaturations with respect to liquid water combined with a condensate supply rate greater than the bulk ice mass diffusional growth rate (Rauber and Tokay 1991), cloud base detrainment that allows for a constant ratio of buoyant consumption of turbulent kinetic energy in the sub-cloud layer to the buoyant production of turbulent kinetic energy within the cloud layer (Liu and Krueger 1998), and/or a mechanism that produces an oscillating vertical velocity (updrafts and downdrafts) to create a periodic evaporation and activation of liquid droplets in the presence of ice particles (Korolev and Isaac 2003).

The 2 Nov cloud maintained itself with a consistent appearance for five hours prior to sunrise. After sunrise, however, the cloud began to change its appearance and break up. It had completely dissipated within three hours of sunrise. Also, the 14 Oct cloud showed evidence of weak convection prior to sunrise. This cloud took on a much more stratiform appearance after sunrise. This shows that solar heating at cloud top, which occurs after sunrise, may significantly alter the morphology of mid-level clouds and lead to what has been termed "post-sunrise dissipation". Given all of the factors that are both trying to maintain and destroy the clouds, and the tenuous balance that must exist for mid-level clouds to be present, altering any one of these processes (such as the radiative heating profile) may be enough to "kill" mid-level clouds. In the next section, we describe the formation and results of a simple model to determine which of these processes are most important in the life cycle of mid-level clouds.

4.2 Budget of Cloud Liquid and Ice

As mentioned in the previous section, the most important processes in the lifetime of mid-level clouds are subsidence, entrainment, radiation and precipitation. Subsidence forces air parcels down into layers of the atmosphere with higher temperatures, and hence, higher saturation vapor pressures, which then causes evaporation of the liquid droplets and ice particles. Entrainment acts to destroy the cloud by bringing drier air parcels into the cloud, which aids in the evaporation of the liquid droplets and ice particles. Radiation acts to sustain the cloud by increasing the instability of the cloud layer, which increases the vertical motion. Precipitation acts to destroy the cloud by removing water molecules from the cloud layer. A simple model was created similar to that of Larson et al. (2001) to evaluate the relative importance of these processes.

This model evaluates the time rate of change of the domain-averaged specific liquid water content, q_l. Since the specific ice water content was generally an order of magnitude less than the specific liquid water content, the effects of the ice phase are ignored, except insofar as ice particles remove water through precipitation. Only in analysis of the North Platte section of the 19 Oct cloud do we run into trouble by this assumption. The change in q_l is assumed to be due to subsidence, S, entrainment, E, radiation, R, and precipitation, P in a linear fashion:

$$\frac{dq_l}{dt} = S + E + R + P \tag{4.1}$$

We assume that the clouds are saturated with respect to liquid water. Then we may write the subsidence term as

$$S = -\rho w g \left(\frac{\partial q_l}{\partial p} \right)_{\theta_l, q_t} \tag{4.2}$$

where ρ is the density of air, w is the vertical velocity, g = 9.8 m s^{-2} is the gravitational acceleration, θ_l is the liquid potential temperature and q_t is the total specific water content. Here we use the approximation

$$\theta_l \cong \theta - \frac{L_v}{c_p} w_l \tag{4.3}$$

where θ is the potential temperature, L_v is the latent heat of vaporization, c_p is the specific heat capacity of dry air at constant pressure and $w_l = q_l/(1-q_l)$ is the liquid water mixing ratio. The total specific water content is the sum of the specific liquid water content and specific water vapor content:

$$q_t = q_l + q_v \tag{4.4}$$

since we neglect the ice phase. Assuming the cloud processes are all adiabatic and reversible, the liquid potential temperature and total specific water content are constant with height, so (4.2) simplifies to

$$S = -\rho w g \frac{dq_l}{dp} \tag{4.5}$$

The entrainment drying term is then given by

$$E = \frac{w_e \Delta q_t}{h} \frac{dq_l}{dq_t} + \frac{w_e \Delta \theta_l}{h} \frac{dq_l}{d\theta_l} \tag{4.6}$$

where h is the cloud depth, w_e is the entrainment velocity, Δq_t is the difference between q_t just above and just below cloud top and $\Delta\theta_l$ is the analogous difference for θ_l. The radiative cooling term is

$$R = \dot{Q} \frac{dq_l}{d\theta_l} \left(\frac{p_0}{p} \right)^{\frac{R_d}{c_p}} \tag{4.7}$$

where $\dot{Q}$ is the net radiative heating or cooling rate, p_0 = 1000 mb, and R_d is the gas constant for dry air. The precipitation term is calculated using

$$P = \frac{\sum_j N_j m_j v_{t,j}}{\rho h} \tag{4.8}$$

where the sum is performed over the all ice particle size bins. The concentration of particles in each size bin is N_j, and each particle in that size bin has mass m_j and terminal velocity $v_{t,j}$.

Profiles of all of the various variables used in these equations were averaged over 30 m thick layers in the vertical and used to calculate S, E, R and P for each layer. These layer-averaged values were averaged over the entire depth of the cloud to determine the cloud-averaged subsidence, entrainment, radiation and precipitation terms.

The set of equations (4.5) - (4.8) assume that the cloud processes are reversible and adiabatic, and assume that horizontal advection can be neglected. The first assumption is validated if the liquid potential temperature and total specific water content are constant with height (pressure). The values of θ_l were found to be constant with height to within 8% in these clouds. The values of q_t, however, varied by 20 - 80% within the clouds. The second assumption is validated as long as we are only looking at one cloud parcel and following it as it moves or if the cloud is horizontally homogeneous and its horizontal extent is much greater than the distance over which the cloud moves during sampling. Lagrangian flight spirals were not used to collect data in any of the clouds presented here, except insofar as the aircraft remained in the cloud volume as the cloud drifted with the wind. Thus we may say we are looking at one substantial air parcel, or the cloud is horizontally homogeneous. Implicit in the results presented in Chapter 3 is the assumption that the clouds are horizontally homogeneous, so we simply keep that assumption here. The horizontal extents of these clouds were much greater than the

distance over which the clouds drifted during sampling. It should also be noted that radiation is not an adiabatic process. The adiabatic assumption is only used to simplify the derivative in (4.7) from $\left(\frac{\partial q_l}{\partial \theta_l}\right)_{q_t,p}$ to $\frac{dq_l}{d\theta_l}$.

The calculation of the subsidence drying term in (4.5) also assumes that the hydrostatic equation holds (i.e. the gravitational pull on the air parcels balances the pressure gradient force, which is trying to lift the parcels). Vertical velocities in these clouds were, for the most part, less than 1 m s^{-1}, so this assumption does not lead to significant errors.

Calculation of the entrainment term in (4.6) requires determination of the entrainment velocity, w_e, and the differences between the in-cloud and above cloud total specific water content and liquid potential temperature, Δq_t and $\Delta \theta_l$. The latter were calculated by first determining cloud top. Then values of q_t and θ_l from the second layer below cloud top were subtracted from similar values from the second layer above cloud top to give values of Δq_t and $\Delta \theta_l$. The entrainment velocity was calculated using the flux jump method. Here we define the entrainment velocity to be

$$w_e = -\frac{\overline{w' q_t'}}{\Delta q_t} \tag{4.9}$$

where the overbar denotes a horizontal average and a prime denotes a departure from the horizontal average. Horizontal averages of w and q_t were calculated using level flight legs near cloud top and used to calculate $\overline{w' q_t'}$. Typically, more than one level flight leg was executed near cloud top. The final value of w_e is then the average of the values from each of these flight legs. Leg lengths varied between 52 km and 218 km, which is

sufficient to reduce the errors to less than 10% (see Lenschow et al. 1994). Table 4.1 shows the values of w_e, Δq_t and $\Delta\theta_l$ for each of the CLEX-9 clouds presented here.

Table 4.1. Values of w_e, Δq_t anc $\Delta\theta_l$ for each of the CLEX-9 clouds presented in this study.

Date	w_e (cm s^{-1})	Δq_t (kg kg^{-1})	$\Delta\theta_l$ (K)
14 Oct	3.8	-5.1×10^{-5}	0.03
19 Oct North Platte	4.1	-1.9×10^{-4}	0.87
19 Oct McCook	7.9	-2.2×10^{-4}	0.92
22 Oct	3.1	-1.3×10^{-4}	2.1
31 Oct	-0.7	-8.2×10^{-5}	0.49
2 Nov	2.0	-1.8×10^{-4}	0.89

The precipitation term (equation 4.8) was calculated using the methods of Heymsfield et al. (2002). The modified gamma distributions (see section 2.3) were divided into 100 μm diameter size bins. For simplicity and because it was the most common particle habit, the particles were all assumed to be aggregates. The average concentration of particles in each size bin, N_j, was calculated. Each particle is assumed to have the same diameter as the other particles in the same size bin. Then the mass of each particle in the jth size bin, m_j, is given by

$$\frac{m_j}{a_j} = \frac{2\rho_e D_j}{3a_r} \tag{4.10}$$

where a_j is the cross-sectional area of the particle (i.e. the area of a circle with diameter D_j multiplied by the cloud-averaged area ratio, a_r) and ρ_e is the cloud-averaged effective density. The Best number is given by

$$X = \frac{4gka_r^{(n-1)}D^3}{3\rho\nu^2} \tag{4.11}$$

The values of n and k depend on particle habit. For aggregates, n = 1.5 and k = 0.015 (Heymsfield et al. 2002). The kinematic viscosity of air, ν, was taken from values reported by Montgomery (1947). The Best number is used to determine the values of the coefficients a_f and b_f, from which the terminal velocity of particles in the jth bin is determined:

$$v_{t,j} = a_f \nu^{(1-2b_f)} D^{(2b_f-1)} \left(\frac{2gm_j}{a_j} \right)^{b_f} \tag{4.12}$$

The relationship between the Best number and the values of a_f and b_f is given in Heymsfield et al. (2002).

The results of this model are shown in Table 4.2. Positive values mean that the physical process is acting to increase the lifetime of the cloud. The fact that the subsidence term is generally positive is indicative that lift, and not subsidence, was occurring. Since the data used in these calculations comes from the entire in-cloud portion of each flight, it is not surprising that the cloud averaged vertical velocity, and hence, the subsidence term is positive. The reasons for the values of the entrainment term from the 31 Oct cloud and the radiation term from the 22 Oct cloud are not well known. The 31 Oct cloud was the only cloud to have a negative value for the entrainment velocity, which is the reason for the positive entrainment term. Since the value of Δq_t for this cloud is negative, the negative entrainment velocity is due to the fact that w' and q_t' are negatively correlated. This is the only cloud where this is true and the reason for this is not known. It may be related to the fact that this cloud was orographically produced and had the form of a set of wave clouds. The negative value of

the radiation term for the 22 Oct cloud is due to the fact that $\dot{Q}$ is negatively correlated with $dq_l / d\theta_l$. Again, this is only true in this cloud. If we instead use the cloud-averaged value of the net radiative heating rate at all levels so that the calculation of the cloud-averaged radiation term is no longer weighted, we find that the radiation term for the 22 Oct cloud has a value of 3.57×10^{-10} kg kg^{-1} s^{-1}.

Table 4.2. Calculated values of the cloud-averaged subsidence, entrainment, radiation and precipitation terms for the CLEX-9 clouds.

Date	Subsidence (kg kg^{-1} s^{-1})	Entrainment (kg kg^{-1} s^{-1})	Radiation (kg kg^{-1} s^{-1})	Precipitation (kg kg^{-1} s^{-1})
14 Oct	2.07×10^{-8}	-1.52×10^{-8}	1.92×10^{-10}	0
19 Oct North Platte	3.63×10^{-8}	-6.39×10^{-10}	4.83×10^{-10}	-1.43×10^{-8}
19 Oct McCook	3.63×10^{-8}	-9.5×10^{-9}	1.92×10^{-10}	0
22 Oct	-2.94×10^{-8}	-2.32×10^{-9}	-2.06×10^{-9}	-5.65×10^{-8}
31 Oct	-3.65×10^{-8}	8.41×10^{-11}	1.23×10^{-9}	-1.06×10^{-8}
2 Nov	3.32×10^{-8}	-9.26×10^{-10}	6.46×10^{-10}	-4.08×10^{-9}

Despite the limitations of this simple model, it is clear that, from an order of magnitude standpoint, the subsidence term is the most important term affecting the lifetime of these mid-level clouds, followed closely by precipitation. The radiation and entrainment terms are typically 1-2 orders of magnitude less. The radiation term increases if the net radiative heating rate profile from before sunrise is used, which shows again that solar heating reduces the instability produced by the net heating profile, although the radiation term is never as large as the subsidence or precipitation terms. This suggests that it is the passage of potential vorticity anomalies or the presence or absence of favorable dynamics that drives the life cycle of these mid-level

clouds. As mentioned above, four of the five clouds formed in areas of PVA. This is the most likely source of lift for these clouds. It is therefore reasonable to assume that the passage of the vorticity anomaly, which would then put the cloud in an area of NVA, is the primary source of subsidence and the most likely process responsible for the death of these clouds. The precipitation term is typically the same order of magnitude as the subsidence term, although the formulation of this term neglects the vertical velocity of the air, which would reduce the terminal velocity of the ice particles relative to the ground. None of these clouds were observed to completely glaciate, so it seems that subsidence is the more important process.

Several clouds experienced "post-sunrise dissipation". This may be due to the fact that the rising of the sun is coincident with the cloud passing from a region of PVA to a region of NVA. The solar heating at cloud top then reduces the ability of radiation to sustain the updrafts when the transition from PVA to NVA occurs, so that the subsidence wins out over the radiation and the cloud dissipates. The results of this simple model suggest this is the case, although a more detailed look into these processes is required to know for sure.

5. Conclusions

5.1 Discussion of Results

In the previous chapters, we have presented the observations made by the University of Wyoming King Air research aircraft as it flew through five mid-level clouds in the fall of 2001 as part of the Ninth Complex Layered Cloud Experiment. One of these clouds was separated into two geographically and microphysically different sections, one being mixed-phase and multi-layered with the highest ratio of ice to liquid, and the other being a single layer comprised only of liquid droplets. Of the remaining four clouds, all were single-layer clouds and three were mixed-phase. Cloud depths varied between 248 m and 3106 m, although most of the clouds were less than 700 m thick.

Profiles of the liquid and ice water contents showed that the maximum liquid water contents were observed in the mid- to upper portions of the single layer clouds, and that the maximum ice water contents were observed near cloud base. This is consistent with the fact the ice particles were growing due to the Wegener-Bergeron-Findeisen mechanism and aggregation, falling through the clouds as they grew, and reaching their maximum size near cloud base. The multi-layered cloud had an ice water content profile that was more nearly uniform with height, especially in the lower layer, suggesting that a possible seeder-feeder mechanism was promoting the formation of ice particles throughout the depth of the layer.

Profiles of radiative and latent heating rates revealed that, in four of the five clouds, a net heating occurred at cloud base and a net cooling occurred at cloud top. This was primarily due to the absorption and emission of longwave radiation by the cloud particles. Latent heating was found be a maximum at the heights where the maximum liquid water content occurred. The multi-layered cloud system, which was comprised mostly of ice, experienced a net cooling at all levels of the cloud.

Profiles of temperature and water vapor mixing ratio were shown. Only two of the five clouds had cloud top inversions of larger than 2 °C. The remaining clouds had no significant inversions at cloud top. Temperatures in-cloud ranged from +2 °C to –25 °C. The liquid-only clouds existed at temperatures between –13 °C and –22 °C. Profiles of the water vapor mixing ratio revealed that only one cloud existed beneath a significant discontinuity in water vapor mixing ratio, with much drier air aloft. The remaining clouds had no significant discontinuities in water vapor mixing ratio at cloud top.

Ice particle size distributions were presented and gave evidence that aggregation was occurring in each of the mixed-phase clouds, to varying degrees. These size distributions provided more evidence that the deeper clouds contained larger ice particles. High concentrations of small ice particles generally existed near cloud top, and low concentrations of large particles generally existed near cloud base. These factors are consistent with growth by aggregation and the Wegener-Bergeron-Findeisen mechanism.

A table of cloud properties that is useful for remote sensing and modeling purposes was presented. This data shows that there is a significant amount of variability in the total optical depths of these clouds. Calculation of the ice particle effective radii revealed that the thicker clouds contained larger ice particles. The variation in liquid droplet effective radius was much less, and not directly related to cloud depth. Domain-averaged liquid water contents were at least a factor of five larger than the domain-

averaged ice water contents, except in the multi-layered cloud system where the two quantities were similar in magnitude.

A simple model was created similar to Larson et al. (2001) to evaluate the relative importance of subsidence, entrainment, radiation and precipitation on the lifetime of these clouds. Generally speaking, the subsidence term was the largest in magnitude, followed closely by the precipitation term. The radiation term (calculated using a solar angle of that near the end of the aircraft sampling period) was typically two orders of magnitude smaller than that subsidence and precipitation terms. When pre-sunrise net radiative heating profiles were used, the magnitude of the radiation terms increased, although they were never as large in magnitude as the subsidence and precipitation terms. The magnitude of the entrainment term was the most variable. In one case it was similar in magnitude to the subsidence term, in another it was three orders of magnitude less.

Four of the five clouds formed in a region of positive vorticity advection. The fifth cloud formed in a region of negative vorticity advection. This cloud was produced by orographic forcing.

The observations made in these five clouds were compared with the results of previous studies of mid-level clouds. Most notably, the results here are very similar to the results of Fleishauer (2001), Tulich and Vonder Haar (1998) and Heymsfield et al. (1991), all of which were studies of continental, North American, mid-level clouds. The results of these studies were examined along with the results of this study to create a consistent picture of mid-level clouds from this geographical region. The combined results yield observations of fifteen mid-level clouds that formed over the Great Plains and Midwest of the United States, and allow for more useful conclusions, which are presented in the next section.

5.2 Conclusions

The generalized results presented in the previous section, combined with the results of Fleishauer (2001), Tulich and Vonder Haar (1998) and Heymsfield et al. (1991) allow us to draw some generalized conclusions about the characteristics of mid-level clouds, as well as the processes involved in their formation, sustenance and dissipation. Mid-level clouds are thin (typically less than 1 km in total depth). Maximum liquid and ice water contents are small (typically less than 0.2 g m^{-3}). Net heating rate profiles are dominated by the absorption and emission of longwave radiation, which leads to a net heating at cloud base and a net cooling at cloud top. The presence of solar and latent heating modifies this profile, but does not change the fact that there is a net heating at cloud base and a net cooling at cloud top. Solar heating reduces the cloud top cooling, but does not cancel it. Latent heating increases the cloud base heating and reduces the cloud top cooling. The diabatic heating and cooling are the largest when the liquid water content is the largest. Liquid droplets absorb more solar radiation than do ice particles, which mostly just scatter the incident solar radiation. Latent heating was dominated by condensation onto the liquid droplets (and not onto the ice particles) due to the fact that liquid droplets were much more numerous than ice particles.

Ice water contents are poorly correlated with temperature. This is due to the fact that ice particles grow by aggregation and vapor deposition and fall through the clouds. They grow the entire time that they are falling through the clouds and reach their largest size at cloud base, just before they exit the cloud and begin to evaporate. This explains why the largest ice particle effective radii were observed in the deepest cloud layers. In multi-layered cloud systems, the ice water content does not typically reach a maximum at cloud base, but is more uniform with height. This is most likely due to seeder-feeder

mechanisms where ice particles fall from the upper layers and trigger ice formation at the tops of the lower layers.

Significant liquid water contents were observed in temperatures as low as –31 °C in previous studies and as low as –25 °C in this study. The clouds that contained negligible amounts of ice particles, and have been referred to as liquid-only clouds, all existed at temperatures below 0 °C. The prevalence of general circulation models and operational forecast models that use temperature cut-offs (such as –20 °C in the case of the CSU GCM) to separate the ice and liquid phases is something that needs to be addressed, as changing the temperature cut-off has been shown to significantly alter the modeled globally averaged outgoing longwave radiation (Fowler and Randall 1996). Mixed-phase clouds are the proof that liquid and ice can coexist, albeit not peacefully.

The primary factors used to forecast the existence of mid-level clouds for this study were the presence of potential vorticity anomalies and significant amounts of moisture in the mid-troposphere. The fact that four of the five clouds in this study formed in regions of positive vorticity advection ahead of the center of the vorticity anomalies gives weight to the theory that the lifetimes of these mid-level clouds were closely linked to the passage of vorticity anomalies. This is supported by the results of the liquid water budget model, which showed that the subsidence term was the most important term affecting cloud lifetime. This may explain why vertical velocities were relatively weak.

Mid-level clouds have been observed to be relatively transient. This is due to the complex balance of processes that are acting to maintain or destroy these clouds. These processes act on the entire spectrum of scales, from the molecular (i.e. liquid and ice particles competing over the available water vapor molecules) to the meso- and synoptic scales (i.e. large regions of upward vertical motion that create these clouds). Convective processes produced by radiation and/or large-scale lift may extend the life of the cloud (if present in moderation) or may mix the cloud right out of existence (if too vigorous). The

moisture that these clouds feed off of cannot come directly from the surface, but only from the remnants of other clouds that existed at midlevels or by sufficient dynamic processes that transport moisture from the boundary layer into the midlevels of the troposphere.

The role of radiation in the morphology of mid-level clouds is complicated. The net heating at cloud base and net cooling at cloud top increase the instability within the cloud layer and act to sustain the clouds. The cloud-top cooling promotes entrainment, however, which acts to destroy the clouds. Several clouds exhibited "post-sunrise dissipation", and this may either be due to the solar heating at cloud top reducing the instability within the cloud layer and, hence, altering the delicate balance that existed prior to sunrise, or the transition of these clouds from a region of positive vorticity advection to a region of negative vorticity advection that, for climatological reasons, happens to coincide with sunrise. The results of the liquid water budget model suggest that radiation is not nearly as important as precipitation and large-scale vertical motion.

5.3 Future Work

This work should in no way be assumed to be an exhaustive study of the properties present in all mid-level clouds, nor of all the processes involved in their formation, sustenance and dissipation. This work does, however, add to the present database of mid-level and mixed-phase clouds. To fully understand mid-level, mixed-phase clouds requires further aircraft studies and/or remote sensing studies, such as the upcoming CLOUDSAT mission (Stephens et al. 2002). These studies should take place in various regions around the globe and under different formation mechanisms. This data should be input into more sophisticated (i.e. time dependent) cloud models to determine the exact roles of subsidence, entrainment, radiation and precipitation in the life of mid-level

clouds. This will allow us to answer the question of whether radiation ultimately acts to maintain these clouds by increasing the instability in the cloud layer or destroy these clouds by promoting cloud-top entrainment.

One property of the atmosphere that is often overlooked in studies of mixed-phase cloud studies is the concentration of ice nuclei. The results of this study, combined with the results of Heymsfield and Miloshevich (1993), suggest that it is the presence or absence of ice nuclei that determines whether or not ice particles will form, especially in clouds warmer than –30 °C. This study, along with most studies of mixed-phase clouds, contained no direct measurements of ice nuclei, so this idea could not be adequately tested. Future studies of mid-level clouds should therefore make an attempt to measure ice nuclei concentrations.

Remote sensing studies, such as CLOUDSAT, will allow for observations of mid-level clouds that occur around the globe. Improved remote sensing techniques should allow for the development of an improved climatology of mid-level clouds using this data. This should also allow for a more quantitative examination of the role of mid-level clouds in climate and allow us to determine if they contribute to global warming or global cooling. The current thought is that mid-level clouds are radiatively neutral, that is, they block as much incoming radiation as outgoing radiation. Further research is needed to test this idea, since the future of our planet's climate is so uncertain and so important for life on earth.

6. References

Baumgartner, D. and M. Spowart, 1990: Evaluation of the Forward Scattering Spectrometer Probe. Part III: Time Response and Laser Inhomogeneity Limitations. *Journal of Atmospheric and Oceanic Technology*, **7**, 666-672.

Bergeron, T., 1935: On the Physics of Clouds and Precipitation. *Proces Verbaux de l'Association de Météorologie, International Union of Geodesy and Geophysics*, Paris, 156-178.

Bohren, C. F. and B. A. Albrecht, 1998: *Atmospheric Thermodynamics*, Oxford University Press, New York, NY, 402 pp.

Bolton, D., 1980: The Computation of Equivalent Potential Temperature. *Monthly Weather Review*, **108**, 1046-1053.

Brenguier, J. L., 1989: Coincidence and Dead-time Corrections for Particle Counters. Part II: High Concentration Measurements with an FSSP. *Journal of Atmospheric and Oceanic Technology*, **6**, 585-598.

Carey, L. D., T. H. Vonder Haar, J. A. Kankiewicz, J. M. Davis, J. M. Forsythe, D. L. Reinke, K. E. Eis, R. P. Fleishauer and V. E. Larson, 2001: An Overview of the Next Complex Layered Cloud Experiment (CLEX-9). Preprint, Battlespace

Atmospheric and Cloud Impacts on Military Operations (BACIMO) Conference, July 10-12, Ft. Collins, CO.

Carey, L. D., T. H. Vonder Haar, J. A. Kankiewicz, J. M. Davis, J. M. Forsythe, D. L. Reinke, K. E. Eis, V. E. Larson and R. P. Fleishauer: The Complex Layered Cloud Experiment. *Bulletin of the American Meteorological Society*, accepted for publication

Cess, R. D., M-H Zhang, G. L. Potter, H. W. Barker, R. A. Colman, D. A. Dazlich, A. D. Del Genio, M. Esch, J. R. Fraser, V. Galin, W. L. Gates, J. J. Hack, W. J. Ingram, J. T. Kiehl, A. A. Lacis, H. Le Treut, X-Z Liang, J. F. Mahouf, B. MaAveney, V. P. Meleshko, J-J Morcrette, D. A. Randall, E. Roeckner, J-F Royer, A. P. Sokolov, P. V. Sporyev, K. E. Taylor, W-C Wang and R. T. Wetherald, 1993: Uncertainties in carbon dioxide radiative forcing in atmospheric general circulation models. *Science*, **262**, 1252-1255.

Clough, S. A., F. X. Kneizys, and R. W. Davies, 1989: Line Shape and the Water Vapor Continuum. *Atmospheric Research*, **23**, 229-241.

Cotton, W. R. and R. A. Anthes, 1989: *Storm and Cloud Dynamics*. Academic Press, pp 745-787.

Cox, S. K., D. S. McDougal, D. A. Randall, and R. A. Schiffer, 1987: FIRE- the First ISCCP Regional Experiment. *Bulletin of the American Meteorological Society*, **88**, 114-118.

Dye, J. E., and D. Baumgardner, 1984: Evaluation of the Forward Scattering Spectrometer Probe. Part I: Electronic and Optical Studies. *Journal of Atmospheric and Oceanic Technology*, **1**, 329–344.

Field, P. R., 1999: Aircraft Observations of Ice Crystal Evolution in an Altostratus Cloud. *Journal of the Atmospheric Sciences*, **56**, 1925-1941.

Findeisen, W., 1938: Kolloid-meteorologische Vorgänge bei Neiderschlags-bildung. *Meteorologische Zeitschrift*, **55**, 121-133.

Fleishauer, R. P., 2001: Observed Microphysical and Radiative Structure of Mid-level, Mixed-phase Clouds. CSU Dissertation, Colorado State University, Ft. Collins, CO, 176 pp.

Fleishauer, R. P., V. E. Larson and T. H. Vonder Haar, 2002: Observed Microphysical Structure of Midlevel, Mixed-Phase Clouds. *Journal of the Atmospheric Sciences,* **59**, 1779-1804.

Fowler, L. D., and D. A. Randall, 1996: Liquid and Ice Cloud Microphysics in the CSU General Circulation Model: Part III. Sensitivity to Modeling Assumptions. *Journal of Climate*, **9**, 561-586.

Fowler, L. D., D. A. Randall and S. A. Rutledge, 1996: Liquid and Ice Cloud Microphysics in the CSU General Circulation Model: Part I. Model Description and Simulated Microphysical Processes. *Journal of Climate*, **9**, 489-529.

Fu, Q. and K. N. Liou, 1992: On the Correlated k-distribution Method for Radiative Transfer in Non-homogeneous Atmospheres. *Journal of the Atmospheric Sciences*, **49**, 2139-2156.

Gabriel, P. M., P. T. Partain and G. L. Stephens, 2001: Parameterization of Atmospheric Radiative Transfer. Part II: Selection Rules. *Journal of the Atmospheric Sciences*, **58**, 3411-3423.

Garrett, T. and P. V. Hobbs, 1999: Calibration of Liquid Water Probes From the University of Washington's CV-580 Aircraft at the Canadian NRC Wind Tunnel. Technical Report for FIRE-ACE/SHEBA Field Project, University of Washington, Seattle, WA, 18 pp.

Gedzelman, S. D., 1988: In Praise of Altocumulus. *Weatherwise*, **41**, 143-149.

Gerber, H., B. G. Arends and A. S. Ackerman, 1994: New Microphysics Sensor for Aircraft Use. *Atmospheric Research*, **31**, 235-252.

Gerber, H., Y. Takano, T. J. Garrett and P. V. Hobbs, 2000: Nephelometer Measurements of the Asymmetry Parameter, Volume Extinction Coefficient and Backscatter Ratio in Arctic Clouds. *Journal of the Atmospheric Sciences*, **57**, 3021-3034.

Harrington, J. Y., T. Reisin, W. R. Cotton, S. M. Kreidenweis, 1999: Cloud Resolving Simulations of Arctic Stratus Part II: Transition-Season Clouds. *Atmospheric Research*, **51**, 45-75.

Heymsfield, A. J., S. Lewis, A. Bansemer, J. Iaquinta, L. M. Miloshevich, M. Kajikawa, C. Twohy and M. R. Poellot, 2002: A General Approach for Deriving the Properties of Cirrus and Stratiform Ice Particles. *Journal of the Atmospheric Sciences*, **59**, 3-29.

Heymsfield, A. J. and L. M. Miloshevich, 1993: Homogeneous Ice Nucleation and Supercooled Liquid Water in Orographic Wave Clouds. *Journal of the Atmospheric Sciences*, **50**, 2335-2353.

Heymsfield, A. J., L. M. Miloshevich, A. Slingo, K. Sassen and D. O'C. Starr, 1991: An Observational and Theoretical Study of Highly Supercooled Altocumulus. *Journal of the Atmospheric Sciences*, **48**, 923-945.

Hobbs, P. V. and A. L. Rangno, 1985: Ice Particle Concentrations in Clouds. *Journal of the Atmospheric Sciences*, **42**, 2523-2549.

Hobbs, P. V. and A. L. Rangno, 1998: Microstructures of Low and Middle-Level Clouds Over the Beaufort Sea. *Quarterly Journal of the Royal Meteorological Society*, **124**, 2035-2071.

Hoskins, B. J., M. E. McIntyre and A. W. Robertson, 1985: On the Use and Significance of Isentropic Potential Vorticity Maps, *Quarterly Journal of the Royal Meteorological Society*, **111**, 877-946.

Jones, J. C., 2003: Comparisons of Satellite-derived Cloud Heights with Radar Measurements of Mid-level, Mixed-phase Clouds. CSU Masters Thesis, Colorado State University, Ft. Collins, CO, 66 pp.

Knollenberg, R. G., 1981: Techniques for Probing Cloud Microstructure. *Clouds, Their Formation, Optical Properties and Effects*, P. V. Hobbs and A. Deepak, Eds., Academic Press, New York, NY, 495pp.

Korolev, A. and G. Isaac, 2003: Phase Transformation of Mixed-phase Clouds. *Quarterly Journal of the Royal Meteorological Society*, **129**, 19-38.

Larson, V. E., R. P. Fleishauer, J. A. Kankiewicz, D. L. Reinke and T. H. Vonder Haar, 2001: The Death of an Altocumulus Cloud. *Geophysical Research Letters*, **28**, 2609-2612.

Lenschow, D. H., J. Mann and L. Kristensen, 1994: How Long is Long Enough for Measuring Fluxes and Other Turbulence Statistics? *Journal of Atmospheric and Oceanic Technology*, **11**, 661-673.

Liu, S. and S. K. Krueger, 1998: Numerical Simulations of Altocumulus Using a Cloud Resolving Model and a Mixed Layer Model. *Atmospheric Research*, **47-48**, 461-474.

McFarquhar, G. M., A. J. Heymsfield, J. Spinhirne and B. Hart, 2000: Thin and Subvisual Tropopause Tropical Cirrus: Observations and Radiative Impacts. *Journal of the Atmospheric Sciences*, **57**, 1841–1853.

Montgomery, R. B., 1947: Viscosity and Thermal Conductivity of Air and Diffusivity of Water Vapor in Air. *Journal of Meteorology*, **4**, 193-196.

Ohtake, T., 1970: Studies on Ice Fog. University of Alaska-Fairbanks Institute of Geophysics Final Report AP-100449.

Paltridge, G. W., W. J. King and C. M. R. Platt, 1986: A Case Study of Ice Particle Growth in a Mixed-Phase Altostratus Cloud. *Australian Meteorology Magazine*, **34**, 149-154.

Pinto, J. O., 1998: Autumnal Mixed-Phase Cloudy Boundary Layers in the Arctic. *Journal of the Atmospheric Sciences*, **55**, 2016-2037.

Rauber, R. M. and A. Tokay, 1991: An Explanation for the Existence of Supercooled Water at the Tops of Cold Clouds. *Journal of the Atmospheric Sciences*, **48**, 1005-1023.

Ritter, B. and J. F. Geleyn, 1992: A Comprehensive Radiation Scheme for Numerical Weather Prediction Models with Potential Applications in Climate Situations. *Monthly Weather Review*, **120**, 303-325

Schiffer, R. A. and W. B. Rossow, 1983: The International Satellite Cloud Climatology Project (ISCCP): The First Project of the World Climate Research Programme. *Bulletin of the American Meteorological Society*, **64**, 779-784.

Starr, D. O'C., 1987: A Cirrus Cloud Experiment: Intensive Field Observations Planned for FIRE. *Bulletin of the American Meteorological Society*, **68**, 119-124.

Stephens, G. L., 1994: *Remote Sensing of the Lower Atmosphere*, Oxford University Press, New York, NY, 523 pp.

Stephens, G. L., P. M. Gabriel and P. T. Partain, 2001: Parameterization of Atmospheric Radiative Transfer. Part I: Validity of Simple Models. *Journal of the Atmospheric Sciences*, **58**, 3391-3409.

Stephens, G. L., S. Tsay, P. W. Stackhouse, P. J. Flatau, 1990: The Relevance of Microphysical and Radiative Properties of Cirrus Clouds to Climate and Climatic Feedback. *Journal of the Atmospheric Sciences*, **47**, 1742-1753.

Stephens, G. L., D. G. Vane, R. J. Boain, G. G. Mace, K. Sassen, Z. Wang, A. J. Illingworth, E. J. O'Connor, W. B. Rossow, S. L. Durden, S. D. Miller, R. T. Austin, A. Benedetti, C. Mitrescu, and the CLOUDSAT Science Team, 2002: The CLOUDSAT Mission and the A-Train: A New Dimension of Space-Based Observations of Clouds and Precipitation. *Bulletin of the American Meteorological Society*, **83**, 1771-1790.

Stephens, G. L. and P. J. Webster, 1979: Sensitivity of Radiative Forcing to Variable Cloud and Moisture. *Journal of the Atmospheric Sciences*, **36**, 1542-1556.

Sun, Z., and K. P. Shine, 1994: Studies of the Radiative Properties of Ice and Mixed-Phase Clouds. *Quarterly Journal of the Royal Meteorological Society*, **120**, 111-137.

Sun, Z., and K. P. Shine, 1995: Parameterization of Ice Cloud Radiative Properties and Its Application to the Potential Climatic Importance of Mixed-Phase Clouds. *Journal of Climate*, **8**, 1874-1888.

Takano, Y. and K. N. Liou, 1995: Radiative Transfer in Cirrus Clouds. Part III: Light Scattering by Irregular Ice Crystals. *Journal of the Atmospheric Sciences*, **52**, 818-837.

Tsonis, A. A., W. R. Leaitch, and M. D. Couture, 1987: The Effect of Calibration of the Forward-Scattering Spectrometer Probe on the Sizing of Cloud Droplets. *Journal of Atmospheric and Oceanic Technology*, **4**, 518–526.

Tulich, S. N. and T. H. Vonder Haar, 1998: Measured and Calculated Structures of a Multi-Layer Altocumulus Cloud. Masters Thesis, CSU Atmos. Sci. Paper #647, Colorado State University, Ft. Collins, CO, 190 pp.

Vonder Haar, T. H., S. K. Cox, G. L. Stephens, J. M. Davis, T. L. Schneider, W. A. Peterson, A. C. Huffman, K. E. Eis, D. L. Reinke and J. M. Forsythe, 1997: Overview and Objectives of the DoD Center for Geosciences Sponsored "Complex Layered Cloud Experiment". Preprints, Cloud Impacts on DoD Operations and Systems Conference, September 23-25, Newport, R.I.

Warren, S. G., C. J Hahn, J. London, R. M. Chervin and R. Jenne, 1988: Global Distribution of Total Cloud Cover and Cloud Type Amount Over Land. NCAR TN-317 STR, 212 pp.

Warren, S. G., C. J Hahn, J. London, R. M. Chervin and R. Jenne, 1988: Global Distribution of Total Cloud Cover and Cloud Type Amount Over the Ocean. NCAR TN-317 STR, 212 pp.

Wegener, A., 1911: *Thermodynamik der Atmosphäre*, Leipzig.

Young, K. C., 1993: *Microphysical Processes in Clouds*, Oxford University Press, New York, NY, pp. 37-39.

Appendix: Calculating Latent Heating Rates

The latent heating rate profiles were calculated as follows. The condensation rate of water vapor molecules per unit surface area, ω, is given by

$$\omega = \frac{\alpha_c e}{\sqrt{2\pi mkT}} \tag{A.1}$$

where α_c= 0.04 is the collection coefficient (Young 1993), e is the vapor pressure calculated by (2.8), m is the mass of a water molecule, k is the Boltzmann constant, and T is temperature. The total surface area of the liquid droplets and ice particles were calculated assuming that all particles have a radius equal to the effective radius. The LWC (IWC) is the mass of liquid (ice) per unit volume of air, which is the mass of liquid (ice) per droplet (particle) multiplied by the number of droplets (particles) per unit volume of air. The mass per droplet, M_l, and mass per particle, M_i, are given by

$$\begin{aligned} M_l &= \frac{4}{3}\rho_l \pi r_{e,l}^3 \\ M_i &= \frac{4}{3}\rho_e \pi r_{e,i}^3 \end{aligned} \tag{A.2}$$

where ρ_l = 1.0 g cm^{-3} is the density of liquid water, ρ_e is the cloud averaged effective density of the ice particles, and $r_{e,l}$ and $r_{e,i}$ are the cloud averaged effective radii of liquid droplets and ice particles, respectively. Then the number of liquid droplets, N_l, and ice particles, N_i, per unit volume of air are given by

$$N_l = \frac{LWC}{M_l}$$
$$N_i = \frac{IWC}{M_i} \tag{A.3}$$

The total surface area of liquid droplets is then

$$A_l = 4\pi r_{e,l}^2 N_l \tag{A.4}$$

The total surface area of the ice particles was calculated as

$$A_i = 4\pi a_r r_{e,i}^2 N_i \tag{A.5}$$

where a_r is the cloud averaged area ratio (see section 2.3). It should be noted that (A.5) is not an exact calculation of the total surface area of the ice particles, as a_r is the ratio of the cross-sectional area of an ice particle to a circle with the same radius. Equation A.5 assumes that the ratio between the total (three-dimensional) surface area of an ice particle to the surface area of a sphere with the same radius is the same as the area ratio. With no knowledge of how the actual surface areas relate to the area ratio, there is no evidence to support this assumption. We argue, however, that using the area ratio to calculate the surface area of the ice particles is more accurate than assuming the ice particles are spherical.

The total mass of water molecules colliding with and condensing on liquid droplets per unit time, M_l, is

$$\mathrm{M}_l = \omega m A_l \tag{A.6}$$

The latent heating rate due to the condensation of this mass of water vapor onto liquid droplets, $Q_{c,l}$, is

$$Q_{c,l} = \frac{\mathrm{M}_l L_c}{\rho_l c_l} \tag{A.7}$$

where L_c is the latent heat of condensation, and c_l is the specific heat capacity of liquid water. Similarly, the latent heating rate due to the condensation of water vapor onto ice particles is

$$Q_{c,i} = \frac{M_i L_s}{\rho_i c_i} \tag{A.8}$$

where L_s is the latent heat of sublimation, c_i is the specific heat capacity of ice, M_i is calculated as in (A.6) by replacing A_l with A_i, and the density of ice, ρ_i, is assumed to be 0.9 g cm^{-3}. The latent heating rate is the sum of the heating rates given by equations (A.7) and (A.8). The latent heats of condensation and sublimation, as well as the specific heat capacities of liquid and ice, vary with temperature. This has not been taken into account, except for the latent heat of condensation. The density of ice is highly variable and changes with temperature, particle habit, the amount of air that is trapped in the lattice structure upon freezing, and the amount of riming. The value of ρ_i chosen is appropriate for pure ice. Since the latent heating of the ice particles was typically an order of magnitude less than that for the liquid droplets, varying the density of ice over the natural range that occurs in cloud particles would have a negligible effect on the overall latent heating rates.